Monthly Notices
of the
ROYAL ASTRONOMICAL SOCIETY

Mon. Not. R. Astron. Soc. **417,** 1534–1558 (2011) doi:10.1111/j.1365-2966.2011.19365.x

The most metal-poor damped Lyα systems: insights into chemical evolution in the very metal-poor regime⋆

Ryan Cooke,[1,2]† Max Pettini,[1,2] Charles C. Steidel,[3] Gwen C. Rudie[3] and Poul E. Nissen[4]

[1]*Institute of Astronomy, Madingley Road, Cambridge CB3 0HA*
[2]*Kavli Institute for Cosmology, Madingley Road, Cambridge CB3 0HA*
[3]*California Institute of Technology, MS 249-17, Pasadena, CA 91125, USA*
[4]*Department of Physics and Astronomy, University of Aarhus, 8000 Aarhus C, Denmark*

Accepted 2011 July 1. Received 2011 July 1; in original form 2011 April 4

ABSTRACT

We present a high spectral resolution survey of the most metal-poor damped Lyα absorption systems (DLAs) aimed at probing the nature and nucleosynthesis of the earliest generations of stars. Our survey comprises 22 systems with iron abundance less than 1/100 solar; observations of seven of these are reported here for the first time. Together with recent measures of the abundances of C and O in Galactic metal-poor stars, we reinvestigate the trend of C/O in the very metal-poor (VMP) regime and we compare, for the first time, the O/Fe ratios in the most metal-poor DLAs and in halo stars. We confirm the near-solar values of C/O in DLAs at the lowest metallicities probed, and find that their distribution is in agreement with that seen in Galactic halo stars. We find that the O/Fe ratio in VMP DLAs is essentially constant, and shows very little dispersion, with a mean $[\langle \mathrm{O/Fe} \rangle] = +0.39 \pm 0.12$, in good agreement with the values measured in Galactic halo stars when the oxygen abundance is measured from the [O I] λ6300 line. We speculate that such good agreement in the observed abundance trends points to a universal origin for these metals. In view of this agreement, we construct the abundance pattern for a typical VMP DLA and compare it to model calculations of Population II and Population III nucleosynthesis to determine the origin of the metals in VMP DLAs. Our results suggest that the most metal-poor DLAs may have been enriched by a generation of metal-free stars; however, given that abundance measurements are currently available for only a few elements, we cannot yet rule out an additional contribution from Population II stars.

Key words: galaxies: abundances – galaxies: evolution – quasars: absorption lines.

1 INTRODUCTION

The initial conditions for cosmic chemical evolution are of fundamental importance to our understanding of galaxy formation and the process of galactic chemical evolution. These conditions, set by the yields of the first few generations of stars, depend on various (largely unknown) factors including the form of the primordial stellar initial mass function (IMF) and the uniformity of the enrichment of the intergalactic medium (IGM; Bromm & Larson 2004; Karlsson, Bromm & Bland-Hawthorn 2011). In order to pin down the initial conditions of cosmic chemical evolution, one should seek to understand the origin and relative abundances of the metals in the least chemically evolved systems.

The most metal-poor damped Lyα absorption systems (DLAs), for example, are usually interpreted as distant protogalaxies at an early stage of chemical evolution (Erni et al. 2006; Cooke et al. 2011). Whilst the origin of their metals is still largely unknown, recent hydrodynamical simulations suggest that such systems might have been enriched by just a few supernova events (Bland-Hawthorn, Sutherland & Karlsson 2011). If this is indeed the case, the most metal-poor DLAs provide a simple route to study the first stages of chemical enrichment in our Universe.

By definition, DLAs have a neutral hydrogen column density in excess of 2×10^{20} H I atoms cm^{-2} (Wolfe et al. 1986; see also the review by Wolfe, Gawiser & Prochaska 2005), which acts to

⋆Based on observations collected at the European Organisation for Astronomical Research in the Southern Hemisphere, Chile [VLT programme IDs 67.A-0078(A), 69.A-0613(A), 083.A-0042(A), 085.A-0109(A)], and at the W.M. Keck Observatory, which is operated as a scientific partnership among the California Institute of Technology, the University of California and the National Aeronautics and Space Administration. The Observatory was made possible by the generous financial support of the W.M. Keck Foundation. Keck telescope time was granted by NOAO, through the Telescope System Instrumentation Program (TSIP). TSIP is funded by NSF.
†E-mail: rcooke@ast.cam.ac.uk

self-shield the gas from the ultraviolet background radiation of quasars (QSOs) and galaxies (Haardt & Madau 2001). This results in the gas having a simple ionization structure subject to negligible corrections for unseen ion stages (Vladilo et al. 2001), quite unlike the Lyα forest clouds that trace the low-density regions of the IGM (e.g. Simcoe, Sargent & Rauch 2004). The main concerns that limit abundance studies in DLAs are line saturation and the possibility that dust may hide some fraction of the metals (Vladilo 2004). These concerns are alleviated when the metallicity of the DLA is below $\sim 10^{-2}$ $Z_{\odot}$, which is also the regime where we expect to uncover the enrichment signature of the earliest generations of stars.

The recent interest in the most metal-poor DLAs (Pettini et al. 2008; Penprase et al. 2010) complements the ongoing local studies of metal-poor stars in the halo of the Milky Way (Cayrel et al. 2004; Beers & Christlieb 2005; Suda et al. 2008; Frebel 2010). These stars are believed to have condensed out of near-pristine gas (perhaps a metal-poor DLA itself?), that was enriched by only a few earlier generations of stars. Thus, the first generation of stars can also be studied through the signature retained in the stellar atmospheres of the most metal-poor stars in the halo of our Galaxy. However, unlike the relative ease with which one can measure the abundances of metal-poor DLAs, deriving element abundances from the stellar atmospheres of metal-poor stars is not straightforward (Asplund 2005). Systematic uncertainties in the derived abundances are introduced by assuming that the spectral line being examined forms in a region that is in local thermodynamic equilibrium (LTE), as well as the need to account for three-dimensional (3D) effects in the 1D stellar atmosphere models.

These effects are particularly acute for oxygen, where several different abundance indicators are known to produce contradictory estimates in the low-metallicity regime (García Pérez et al. 2006). Despite the efforts of many authors, our uncertainty in the derived oxygen abundances has sparked an ongoing debate as to the trend of [O/Fe][1] in the Milky Way when [Fe/H] $\lesssim -1.0$. A history of the relevant discussion on [O/Fe] is provided by McWilliam (1997), with further details given in Section 6.2. In brief, at low metallicity, both O and Fe are produced exclusively by Type-II supernovae (SNe II) and the winds from their progenitors. When [Fe/H] $\gtrsim -1.0$, there is a drop in [O/Fe] due to the *delayed* contribution of Fe from Type-Ia supernovae (SNe Ia). Thus, the [O/Fe] ratio is most commonly used to measure the time delay between SNe II and the onset of SNe Ia. At the lowest metallicity, however, one can use the [O/Fe] ratio as a measure of the relative production of α- to Fe-peak elements by the first few generations of massive stars.

Another key diagnostic ratio at low metallicity that may shed light on the nature of the early generations of stars was uncovered by Akerman et al. (2004) who reported a rather surprising evolution of [C/O] with decreasing O abundance in their sample of 34 halo stars (see also Spite et al. 2005). In disc and halo stars when the oxygen abundance is $\gtrsim -1.0$, [C/O] steadily rises from [C/O] ~ -0.5 to solar. When [O/H] $\lesssim -1.0$, galactic chemical evolution models that *only* consider the nucleosynthetic products of Population II stars predict [C/O] to decrease or plateau, contrary to the observed trend. The increase in [C/O] with decreasing metallicity has thus been interpreted as evidence for an increased carbon yield from either Population III stars (Chieffi & Limongi 2002; Umeda & Nomoto 2003; Heger & Woosley 2010) or rapidly rotating low-metallicity Population II stars (Chiappini et al. 2006). At first, concerns were raised regarding the accuracy of the derived C and O abundances, since the lines used are subject to large non-LTE corrections. Fabbian et al. (2009a), however, performed a non-LTE analysis of the same lines, with further constraints from additional C I lines, to confirm the reality of the stellar [C/O] trend. These results depend somewhat on the adopted cross-sections for collisions of C I and O I atoms with electrons and hydrogen atoms, but for all probable values, [C/O] increases with decreasing metallicity when [O/H] < -2.0.

To summarize, at present there are still some remaining concerns that prevent us from accurately measuring C and O abundances in the atmospheres of metal-poor halo stars. These difficulties have prompted a few teams to focus on very metal-poor[2] (VMP) DLAs where the absorption lines of C II and O I may be unsaturated and the abundances of C and O can be measured with confidence. Unfortunately, these near-pristine DLAs are rare, falling in the tail of the metallicity distribution function of DLAs (Prochaska et al. 2007). Thus, only a handful of confirmed VMP DLAs are known at present. The first high spectral resolution survey [$R \simeq 40\,000$, full width at half-maximum (FWHM) $\simeq 7\,\mathrm{km\,s^{-1}}$] for VMP DLAs was conducted by Pettini et al. (2008), whose specific goal was to study the relative abundances of the CNO group of elements as a probe of early nucleosynthesis. Indeed, this was the first study to independently confirm the increased [C/O] abundance at low metallicity, suggesting that near-solar values of [C/O] are commonplace in this metallicity regime.

The [C/O] trend reported by Pettini et al. (2008) has also been independently noted by Penprase et al. (2010) in a medium spectral resolution ($R \simeq 5000$, FWHM $\simeq 60\,\mathrm{km\,s^{-1}}$) survey of 35 DLAs (a preliminary report of this study can be found in Penprase et al. 2008). In many of their systems, the C II and O I lines were thought to be affected by line saturation, leaving only five DLAs to test the trend in C/O. Interestingly, this sample of DLAs suggests that [C/O] continues to rise to *supersolar* values when [O/H] $\lesssim -3$.

Such surveys for VMP DLAs are most useful for studying the general properties of *entire clouds* of near-pristine gas before they form stars. In this contribution, we build on our ongoing survey for the most metal-poor DLAs as probes of early nucleosynthesis (Pettini et al. 2008; Cooke et al. 2011). With additional systems drawn from the literature, the total sample presented herein amounts to 22 VMP DLAs with abundance measurements derived from high spectral resolution data. From this sample, we confirm the elevated [C/O] values in these systems and, for the first time, present the trend of [O/Fe] in the most metal-poor DLAs. For both of these diagnostic ratios, we comment on the implications our findings have on local studies of Galactic metal-poor halo stars. Finally, we construct the abundance pattern of a typical VMP DLA for the elements C, N, O, Al, Si and Fe, and compare it to model calculations of Population II and Population III nucleosynthesis.

This paper is arranged as follows. In Section 2 we detail the processing and preparation of the data. In Section 3 we explain the profile fitting procedure used for our new sample of VMP DLAs, which are discussed in Section 4. The accuracy of our abundance analysis is discussed in Section 5, before we investigate the behaviour of [C/O] and [O/Fe] in VMP DLAs and compare with stellar data, in Section 6. Finally, we discuss the implications for

[1] We adopt the standard notation: $[\mathrm{A/B}] \equiv \log(N_{\mathrm{A}}/N_{\mathrm{B}}) - \log(N_{\mathrm{A}}/N_{\mathrm{B}})_{\odot}$, where $N_{\mathrm{A,B}}$ refers to the number of atoms in element A and B.

[2] Herein, we adopt 'very metal-poor' to be those DLAs with [Fe/H] < -2.0, in line with the classification scheme for stars proposed by Beers & Christlieb (2005).

Table 1. Journal of observations.

QSO	g^a (mag)	z_{em}	z_{abs}	Telescope/ instrument	Wavelength range (Å)	Resolution (km s^{-1})	Integration time (s)	S/N^b	Programme ID
J0311−1722	17.7	4.039	3.73400	VLT/UVES	4370–6410^c	6.9	3 600	15	69.A-0613(A)^d
J0831+3358	19.5	2.427	2.30364	KECK/HIRESb	3130–5970^c	7.3	18 600	15	A185Hb
J1001+0343	19.2	3.198	3.07841	VLT/UVES	3740–6650^c	7.3	33 700	40	083.A-0042(A)
J1037+0139	19.4	3.059	2.70487	VLT/UVES	3640–6650^c	7.3	26 075	45	083.A-0042(A)
J1340+1106	19.0	2.914	2.50792	VLT/UVES	3483–6652^c	7.3	29 800	50	085.A-0109(A)
			2.79583	VLT/UVES	3483–9396^c	10.3	10 800	40	67.A-0078(A)^d
				KECK/HIRES	4648–7044^c	8.1	8 100	25	U11H^d
J1419+0829	18.9	3.030	3.04973	VLT/UVES	3710–6652^c	7.3	29 800	43	085.A-0109(A)

[a]Magnitudes are SDSS *g* band, except for J0311−1722 (not covered by the SDSS) which is *R* band (Péroux et al. 2001).
[b]Indicative signal-to-noise ratio at 5000 Å (or 6000 Å in the case of J1340+1106).
[c]With some wavelength gaps.
[d]Spectra downloaded from either the UVES or HIRES data archives.[4,5]

our findings in Section 7, before summarizing our main results and drawing our conclusions in Section 8.

2 OBSERVATIONS AND DATA REDUCTION

2.1 Target selection

Even at the relatively low spectral resolution afforded by the Sloan Digital Sky Survey (SDSS), one can easily recognize DLAs in the spectra of quasars, owing to the characteristic damping wings of the Lyα absorption line profile. Subsequent identification of associated metal line absorption leads to a rough estimate of the gas-phase metallicity. Candidate metal-poor DLAs are then identified as those DLAs that appear to exhibit no metal line absorption; these absorption features are unresolved at the spectral resolution of the SDSS. However, when these candidates are re-observed with echelle spectrographs of high resolution ($R \gtrsim 30\,000$, FWHM $\lesssim 10$ kms^{-1}), the metal absorption lines are resolved, and in many cases it is possible to measure elemental abundances with confidence (Pettini et al. 2008).

The most recent trawls through SDSS spectra of ∼8000 quasars with $z_{em} \gtrsim 2.2$ has yielded a sample of ∼1000 DLAs (Noterdaeme et al. 2009; Prochaska & Wolfe 2009), of which ∼400 are classified as 'metal-poor' (Penprase et al. 2010).[3] From compilations such as these, we selected a handful of metal-poor DLA candidates that exhibit *no discernible metal-line absorption* at the spectral resolution of the SDSS, and re-observed these with echelle spectrographs, giving higher priority to candidates with: (i) bright quasars, so as to efficiently obtain spectra with signal-to-noise ratios S/N $\gtrsim 20$ in the continuum; (ii) DLAs where the difference between z_{abs} and z_{em} is minimized so that the absorption lines of interest (e.g. O I λ1302 and C II λ1334) are not blended with unrelated Lyα forest lines; (iii) quasars whose emission redshift is below $z_{em} \lesssim 3.3$, so there is an improved chance that other lines of interest (e.g. O I λ1039 and C II λ1036) are not blended with Lyα forest lines; (iv) DLAs at the low end of the column density distribution function – that are still DLAs – to ensure that even the strongest metal absorption lines are unsaturated, allowing us to measure the metal ion column densities with confidence; and (v) quasars with more than one metal-poor DLA candidate in their spectra.

Our survey to date consists of 12 DLAs with [Fe/H] ≤ −2.0. Initial results for four of these were published by Pettini et al. (2008), while a fifth DLA, showing a pronounced C enhancement relative to Fe, was the subject of a recent study by Cooke et al. (2011). The observations and analysis of the remaining seven DLAs, including one from the European Southern Observatory's (ESO) Ultraviolet and Visual Echelle Spectrograph (UVES) data archive, are presented here. To our own data, we add a collection of published abundance measurements in 10 VMP DLAs, selected as described in Section 4.8, to assemble an overall sample of abundance measurements in 22 VMP DLAs, all obtained from high-resolution spectra ($R \gtrsim 30\,000$).

2.2 Echelle spectroscopic follow-up

In order to achieve the high S/N and spectral resolution required for accurate DLA abundance measurements, we observed our prime candidates with echelle spectrographs on 8–10 m class telescopes. Most of our candidates were observed with the UVES spectrograph (Dekker et al. 2000), which is mounted on UT2 at the Very Large Telescope facility. An additional system was observed with the W. M. Keck Observatory's High Resolution Echelle Spectrometer (HIRES; Vogt et al. 1994) on the Keck I telescope. Table 1 lists details of the observations of seven VMP DLAs reported here for the first time. For J1340+1106, we include details of some additional data, of comparable spectral resolution to ours, retrieved from the ESO[4] and Keck Observatory[5] data archives [programme IDs 67.A-0078(A) and U11H, respectively]. We have also retrieved UVES spectra of the quasar J0311−1722 from the ESO data archive [programme ID 69.A-0613(A); see Péroux et al. 2005], since the metal lines for the VMP DLA along this sightline have not been previously analysed.

Our own UVES observations [programme IDs 083.A-0042(A) and 085.A-0109(A)] employed a 1.2 arcsec wide slit, resulting in a spectral resolution $R \sim 41\,000$ (velocity FWHM ≈ 7.3 km s^{-1}) sampled with ∼3 pixels. We used dichroic 1 to split the quasar light into the blue and red spectroscopic arms containing the HER_5 filter and SHP700 filter, respectively. The resulting central wavelength for each arm was 3900 Å (blue) and 5640 Å (red). Both the blue- and red-sensitive CCDs used 2 × 2 on-chip binning. For our HIRES observations (programme ID A185Hb) we used the C5 decker

[3] In this context, a DLA is classed as 'metal-poor' if it has fewer than three significantly (4σ) detected metal absorption lines at the spectral resolution of the SDSS.

[4] http://archive.eso.org/eso/eso_archive_main.html
[5] https://www2.keck.hawaii.edu/koa/public/koa.php

(a 7.0 × 1.148 arcsec slit) which, with sub-arcsec seeing, gave a spectral resolution of $R \sim 41\,000$ (cf. Cooke et al. 2011), also sampled with ∼3 pixels. We employed the ultraviolet cross-disperser with no filters, and used 2 × 2 on-chip binning.

2.3 Data reduction

We used the standard UVES data reduction pipeline[6] provided by ESO to reduce the UVES data. The UVES reduction pipeline performs the usual steps relevant to echelle data reduction. The preliminary steps include bias subtraction, flat fielding and background subtraction. The echelle orders are then traced using a flat-field frame taken with a pinhole decker, and 1D spectra extracted. The data are wavelength calibrated with reference to a ThAr lamp.

The HIRES data were reduced with the MAKEE data reduction pipeline developed by Tom Barlow. MAKEE performs the same reduction steps as outlined above, but a trace frame is not always readily available. When available, the orders were traced using a flat-field frame taken with a pinhole decker. Otherwise, the science exposure of the quasar itself was used when a satisfactory trace could be made. Failing this, a trace frame was generated with a suite of purpose-built PYTHON programs, using the science frame as a guide to trace the echelle orders.

Following these initial reduction steps, for each object we combined the science exposures using the software package UVES_POPLER,[7] maintained by Michael Murphy. This software merges individual echelle orders, and maps the data on to a vacuum heliocentric wavelength scale. Finally, we normalized the data by dividing out the quasar continuum and emission lines. Using the approximate redshift derived from each DLA's SDSS discovery spectrum, we then prepared the final data for analysis by extracting a $\pm 150\,\mathrm{km\,s^{-1}}$ window around the pixel with highest optical depth near all available absorption lines of interest. Finally, a further fine adjustment to the continuum was applied to these extracted portions of the spectra when necessary.

3 PROFILE FITTING

For DLAs with a metallicity below $1/100\,\mathrm{Z_\odot}$, the metal line absorption is typically concentrated in only a few clouds of low velocity dispersion (Ledoux et al. 2006; Murphy et al. 2007; Prochaska et al. 2008). By assuming that a Maxwellian distribution accurately describes the velocities of the dominant atoms within the neutral cloud, we can model a DLA's absorption lines by a Voigt profile. To this end, we employed the Voigt profile fitting software VPFIT to derive the cloud parameters for all DLAs in our sample.[8]

VPFIT uses a chi-squared minimization algorithm to simultaneously fit multiple Voigt profiles to a set of absorption lines characterized by three free parameters: (1) the cloud's absorption redshift ($z_{\rm abs}$); (2) the Doppler parameter of the absorbing gas (b in $\mathrm{km\,s^{-1}}$); and (3) the column density of the ion that gives rise to the absorption line. When it was evident that the DLA metal absorption arises from more than one cloud component, we introduced additional components to reduce the χ^2 [such that the χ^2 divided by the number of degrees of freedom (d.o.f.) was close to 1.0], whilst maintaining realistic errors on the derived parameters (i.e. $\lesssim$10 per cent uncertainty on b and a redshift uncertainty less than the sampling size of $\sim 2.5\,\mathrm{km\,s^{-1}}$). Throughout the fitting procedure we assumed that the dominant ions in H I regions (e.g. C II, N I, O I, Si II, Fe II) are kinematically associated with the same gas. We therefore fixed the redshift and Doppler parameter of each absorption component to be the same for each of these ions. The resulting cloud model parameters, including the reduced χ^2, are provided in Table 2 where, as a guide, the last column lists the fraction of the total column density of Si II in each component. The total column densities of available ions in each DLA are collected in Table A1. Table 3 lists laboratory wavelengths and oscillator strengths of relevant atomic transitions from the compilation by Morton (2003), with subsequent updates by Jenkins & Tripp (2006).

Table 2. Absorption components of low ion transitions.

Component number	$z_{\rm abs}$	b ($\mathrm{km\,s^{-1}}$)	Fraction[a] N(Si II)
J0311−1722: DLA at $z_{\rm abs} = 3.73400$, χ^2/d.o.f. = 0.80			
1	3.733862 ± 0.000017	5.6 ± 1.2	0.18
2	3.733998 ± 0.000007	2.7 ± 0.8	0.23
3	3.734035 ± 0.000028	14.4 ± 1.5	0.20
4	3.734439 ± 0.000002	4.6 ± 0.2	0.39
J0831+3358: DLA at $z_{\rm abs} = 2.30364$, χ^2/d.o.f. = 1.20			
1	2.303565 ± 0.000004	4.4 ± 0.2	0.49
2	2.303720 ± 0.000004	6.1 ± 0.3	0.51
J1001+0343: DLA at $z_{\rm abs} = 3.07841$, χ^2/d.o.f. = 1.42			
1	3.078413 ± 0.000002	7.0 ± 0.1	1.00
J1037+0139: DLA at $z_{\rm abs} = 2.70487$, χ^2/d.o.f. = 1.08			
1	2.704870 ± 0.000002	5.9 ± 0.2	1.00
J1340+1106: DLA at $z_{\rm abs} = 2.50792$, χ^2/d.o.f. = 1.38			
1	2.507649 ± 0.000003	2.0 ± 0.4	0.19
2	2.507921 ± 0.000001	5.8 ± 0.1	0.81
J1340+1106: DLA at $z_{\rm abs} = 2.79583$, χ^2/d.o.f. = 1.76			
1	2.7955454 ± 0.0000018	9.2 ± 0.1	0.21
2	2.7958272 ± 0.0000007	6.55 ± 0.05	0.79
J1419+0829: DLA at $z_{\rm abs} = 3.04973$, χ^2/d.o.f. = 1.45			
1	3.049649 ± 0.000002	3.5 ± 0.1	0.43
2	3.049835 ± 0.000002	6.4 ± 0.1	0.57

[a]Fraction of the total column density of Si II.

4 INDIVIDUAL OBJECTS

In this section, we briefly comment on the properties of each new DLA analysed in this paper.

4.1 J0311−1722: DLA at $z_{\rm abs} = 3.73400$

The VMP DLA along the line-of-sight to J0311−1722 (J2000.0: $03^{\rm h}11^{\rm m}15\overset{\rm s}{.}20$, $-17^\circ 22' 47\overset{''}{.}4$) was first identified by Péroux et al. (2001). Follow-up UVES spectroscopy by Péroux et al. (2005) revealed an Lyα absorber at $z_{\rm abs} = 3.734$ with $\log\ [N(\mathrm{H\,I})/\mathrm{cm^{-2}}] = 19.48 \pm 0.10$, which is lower than the conventional limit for DLAs set by Wolfe et al. (1986), $\log\,[N(\mathrm{H\,I})/\mathrm{cm^{-2}}] \geq 20.3$. Such systems are often referred to as sub-DLAs (Péroux et al. 2003a)

[6] We used version 4.3.0, available from: http://www.eso.org/sci/software/pipelines/

[7] UVES_POPLER can be downloaded from http://astronomy.swin.edu.au/∼mmurphy/UVES_popler

[8] VPFIT is available from http://www.ast.cam.ac.uk/∼rfc/vpfit.html

Table 3. Adopted metal line laboratory wavelengths and oscillator strengths.

Ion	Wavelength (Å)	f	Ion	Wavelength (Å)	f	Ion	Wavelength (Å)	f
C II	1036.3367	0.118	Al II	1670.7886	1.740	Fe II	1063.1764	0.0547
C II	1334.5323	0.1278	Al III	1854.71829	0.559	Fe II	1081.8748	0.0126
C II*	1335.6627	0.01277	Al III	1862.79113	0.278	Fe II	1096.8769	0.0327
C II*	1335.7077	0.115	Si II	989.8731	0.171	Fe II	1125.4477	0.0156
N I	1134.4149	0.0278	Si II	1020.6989	0.0168	Fe II	1143.2260	0.0192
N I	1134.9803	0.0416	Si II	1190.4158	0.292	Fe II	1144.9379	0.0830
N I	1199.5496	0.1320	Si II	1193.2897	0.582	Fe II	1260.533	0.0240
N I	1200.2233	0.0869	Si II	1260.4221	1.18	Fe II	1608.4509	0.0577
N I	1200.7098	0.0432	Si II	1304.3702	0.0863	Fe II	1611.20034	0.00138
N II	1083.9937	0.111	Si II	1526.7070	0.133	Fe II	2344.21296	0.1142
O I	925.446	0.000354	Si II	1808.01288	0.00208	Fe II	2374.46033	0.0313
O I	936.6295	0.00365	S II	1250.578	0.00543	Fe II	2382.76418	0.320
O I	948.6855	0.00631	S II	1253.805	0.0109	Ni II	1317.217	0.057
O I	976.4481	0.00331	S II	1259.5180	0.0166	Ni II	1370.132	0.056
O I	988.5778	0.000553	Ar I	1048.2199	0.263	Ni II	1454.842	0.0323
O I	988.6549	0.0083	Ar I	1066.6598	0.0675	Ni II	1709.6042	0.0324
O I	988.7734	0.0465	Cr II	2056.25693	0.1030	Ni II	1741.5531	0.0427
O I	1039.2304	0.00907	Cr II	2062.23610	0.0759	Ni II	1751.9157	0.0277
O I	1302.1685	0.048						

or super Lyman-limit systems, and are defined to have $19.0 \leq \log\,[N(\mathrm{H\,I})/\mathrm{cm}^{-2}] \leq 20.3$.

Péroux et al. (2005) derived their estimate of $N(\mathrm{H\,I})$ for this absorber from a consistent model fit (with $b = 39.3\,\mathrm{km\,s}^{-1}$; Péroux, private communication) to the first six Lyman lines (from Lyα to Ly6), where the Lyα line produces the poorest fit. Having re-analysed these data, giving higher priority to the Lyα and Lyβ lines, we find that a better fit results if $\log\,[N(\mathrm{H\,I})/\mathrm{cm}^{-2}] = 20.30 \pm 0.06$ (see top panel of Fig. 1), provided that the Doppler parameter is $b \lesssim 30\,\mathrm{km\,s}^{-1}$.

In the lower panels of Fig. 1 we present a selection of the metal lines associated with this VMP DLA. All of the available metal absorption lines are unsaturated, leading to reliable estimates of the metal column densities. A four-component model was found to accurately reproduce the metal-line profiles, whilst maintaining reasonable estimates of the parameter errors (see Section 3). The derived cloud model parameters are listed in Table 2. Although both C II lines (λ1334 and λ1036) are blended on the red wing of component 4 (centred near $v = 0\,\mathrm{km\,s}^{-1}$ in Fig. 1), this does not greatly affect our final estimate of $N(\mathrm{C\,II})$, since component 4 has a well-determined Doppler parameter from the relative strengths of Si II λ1260 and Si II λ1304, and from other unblended transitions in regions of high S/N. In any case, the majority of the absorbing column is contributed by the first three components (∼60 per cent). We list the total column density returned by VPFIT for each available ion in Table 4.

In this table, we also provide upper limits for the column densities of several key ions that are undetected at the S/N of the data. Specifically, we calculate the 3σ limiting rest-frame equivalent width, W_0, over the velocity interval of absorption exhibited by the weakest transition, which in this case is Si II λ1304. A 3σ upper limit to the undetected feature is then derived using the optically thin limit approximation, $N = 1.13 \times 10^{20} \cdot W_0/\lambda^2 f\ \mathrm{cm}^{-2}$. For N I we use the undetected λ1200.2 line to derive $W_0(\mathrm{N\,I}) \leq 13\,\mathrm{m\AA}$, which implies $\log N(\mathrm{N\,I})/\mathrm{cm}^{-2} \leq 13.07$. Similarly for Fe II λ1125, $W_0(\mathrm{Fe\,II}) \leq 10\,\mathrm{m\AA}$ implies $\log N(\mathrm{Fe\,II})/\mathrm{cm}^{-2} \leq 13.76$.

4.2 J0831+3358: DLA at $z_{\mathrm{abs}} = 2.30364$

We observed J0831+3358 with HIRES on 2009 December 9 under good conditions with sub-arcsec seeing. We used a 1.148 arcsec wide slit which, as measured by Cooke et al. (2011), delivered a spectral resolution of $7.3\,\mathrm{km\,s}^{-1}$ FWHM. Unfortunately, the Lyα line at $\lambda_{\mathrm{obs}} \simeq 4015$Å falls in a gap between two of the CCDs on the HIRES detector mosaic. Thus, for this DLA, we adopt the H I column density $\log[N(\mathrm{H\,I})/\mathrm{cm}^{-2}] = 20.25 \pm 0.15$ derived by Penprase et al. (2010) from their observations of this QSO at $R \simeq 5000$, which is sufficient to resolve the broad damped profile of the Lyα line.

The metal lines in our data are well fit by a model with two components of roughly equal strength separated by $14\,\mathrm{km\,s}^{-1}$ (see Fig. 2). Details of the derived cloud model are presented in Table 2, with the associated column densities given in Table 5. The C II lines are saturated in this DLA, however, we have a clean measurement of $N(\mathrm{O\,I})$ from a number of unsaturated O I lines. In Table 5 we also provide 3σ upper limits to the N I and S II column densities which are undetected at the S/N of our data.

4.3 J1001+0343: DLA at $z_{\mathrm{abs}} = 3.07841$

This QSO was observed with UVES in service mode on the nights of 2009 April 19 and 29, 2010 January 11 and 27, and 2010 February 7. Our total integration time was 33 700 s, yielding an S/N per pixel of ∼40 at 5000 Å. The DLA inline to J1001+0343 was also investigated by Penprase et al. (2010), being amongst the most metal-poor in their sample. From our observations we derive an H I column density of $\log[N(\mathrm{H\,I})/\mathrm{cm}^{-2}] = 20.21 \pm 0.05$ from the wings of the Lyα absorption line. This compares well with the estimate by Penprase et al. (2010), $\log[N(\mathrm{H\,I})/\mathrm{cm}^{-2}] = 20.15 \pm 0.10$. We present our Voigt profile fit to the Lyα line in the top panel of Fig. 3.

The remaining panels of Fig. 3 showcase a number of the available absorption lines that were used in deriving the cloud model.

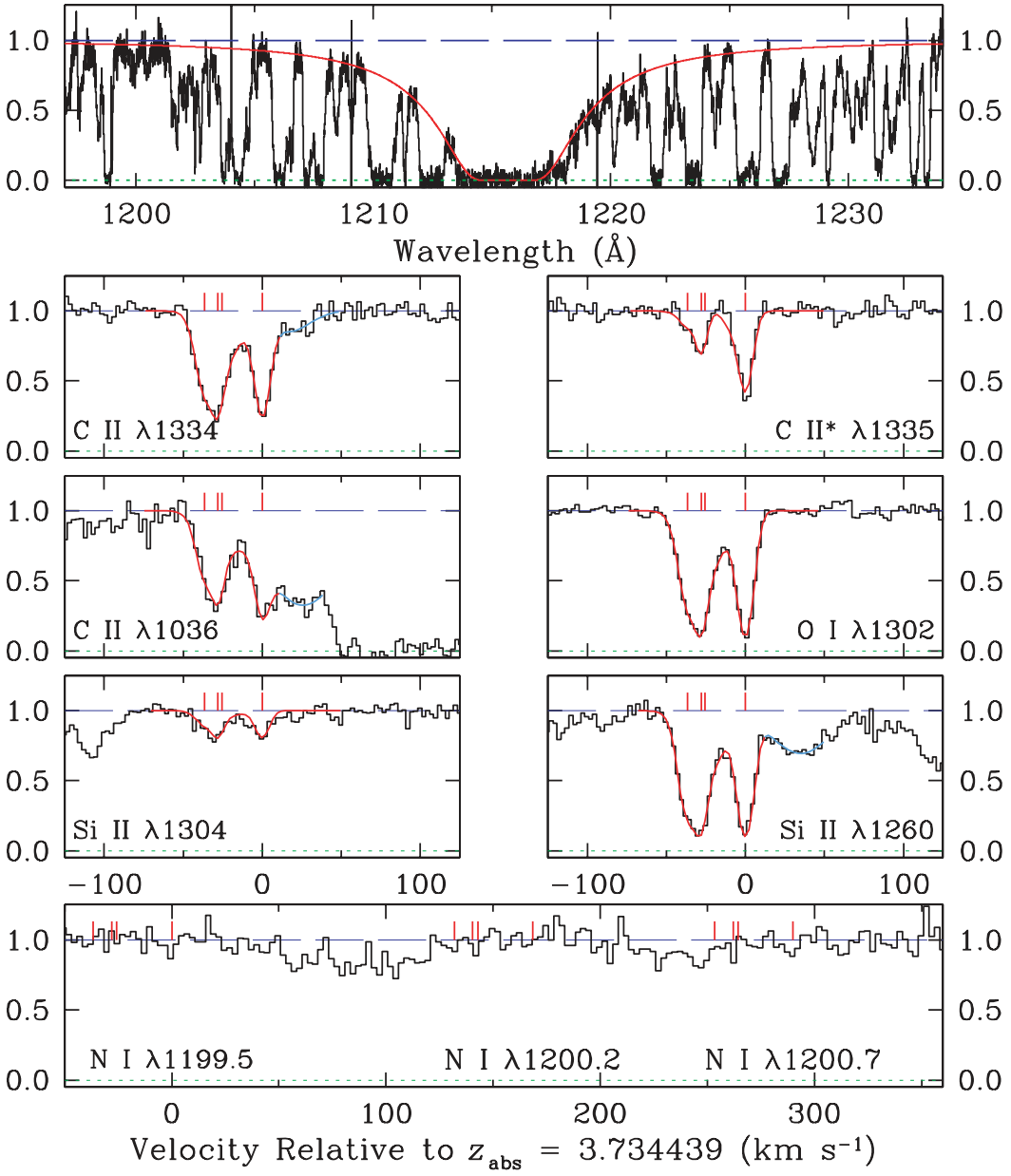

Figure 1. The top panel shows the DLA towards J0311−1722 (black histogram) which exhibits a damped Lyα line at $z_{abs} = 3.73400$. The red continuous line shows the theoretical Voigt profile for a neutral hydrogen column density $\log[N(\mathrm{H\,I})/\mathrm{cm}^{-2}] = 20.30$. The remaining panels display a selection of metal lines, overlaid with the Voigt profiles for the derived cloud model (in red) and blends (in light blue). The red tick marks above the normalized continuum indicate the locations of the absorption components. For all panels, the *y*-axis scale is residual intensity. The normalized quasar continuum and zero-level are shown by the blue dashed and green dotted lines, respectively.

Table 4. Ion column densities of the DLA in J0311−1722 at $z_{abs} = 3.73400$.

Ion	Transitions used	$\log N(\mathrm{X})/\mathrm{cm}^{-2}$
H I	1025, 1215	20.30 ± 0.06
C II	1036, 1334	14.02 ± 0.08
C II*	1335	13.55 ± 0.06
N I	1200.2	$\leq 13.07^a$
O I	1302	14.70 ± 0.08
Si II	1260, 1304	13.31 ± 0.07
Fe II	1125	$\leq 13.76^a$

[a] 3σ limiting rest-frame equivalent width.

In fact, all of the available metal absorption lines are unsaturated in this DLA, thus providing reliable measurements of the elemental abundances. Several metal-line transitions of varying strength are well fit by a single component cloud model with a Doppler parameter of $b = 7.0 \pm 0.1\,\mathrm{km\,s^{-1}}$ (see Table 2). The curve of growth analysis by Penprase et al. (2010) yielded a Doppler parameter of $7.5\,\mathrm{km\,s^{-1}}$, which is in good agreement with that found here. The derived column densities for all available ions are presented in Table 6. We also provide 3σ upper limits to the N I and S II column densities which are undetected at the S/N of our data. Fe II λ1608 is detected at the 3.6σ level. The corresponding fit is presented in the bottom-right panel of Fig. 3 (note the different *y*-axis scale).

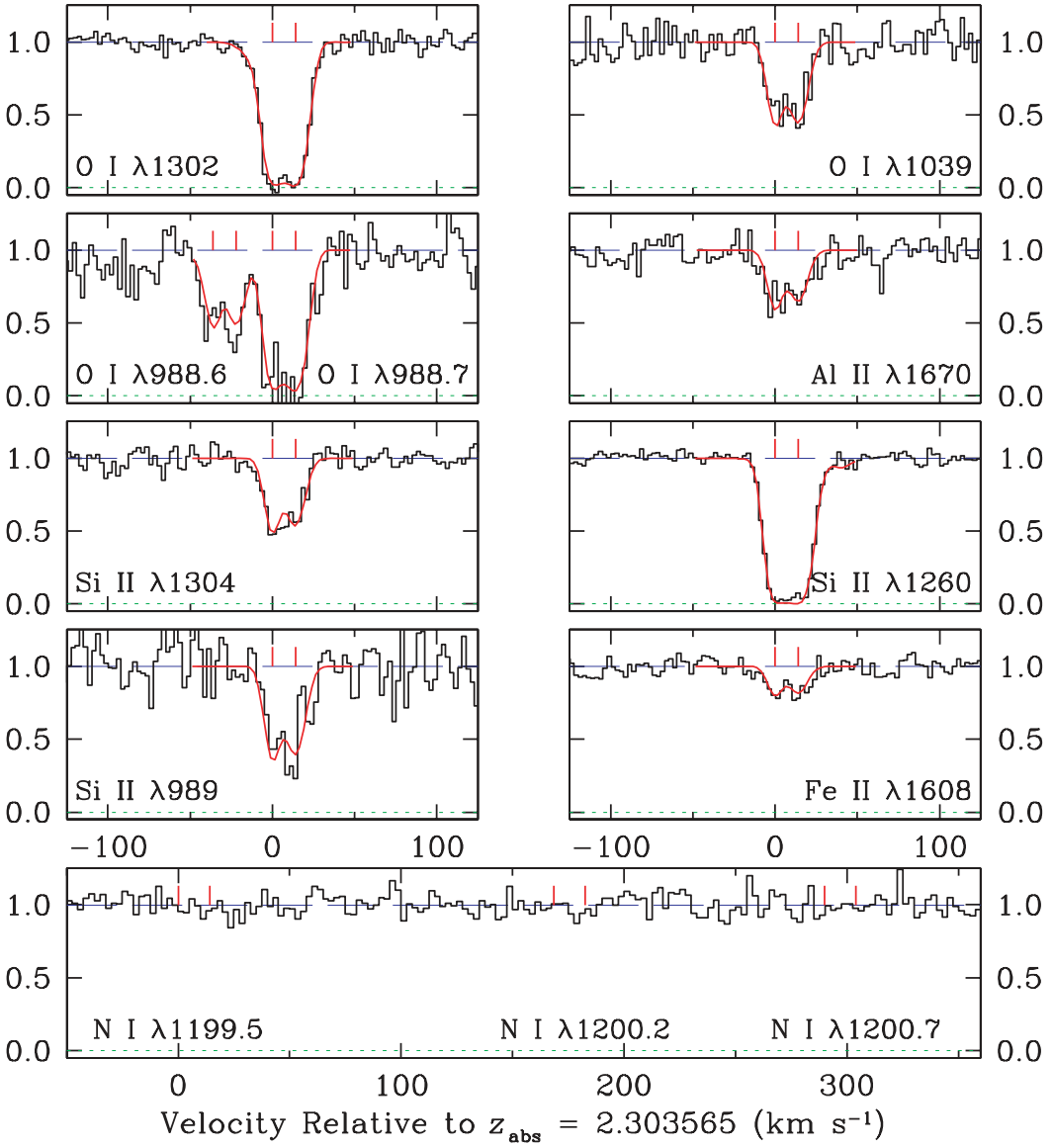

Figure 2. Same as Fig. 1 for a selection of metal lines associated with the $z_{abs} = 2.30364$ DLA towards J0831+3358.

Table 5. Ion column densities of the DLA in J0831+3358 at $z_{abs} = 2.30364$.

Ion	Transitions used	log N(X)/cm^{-2}
H I	1215	20.25± 0.15[a]
N I	1199.5	≤12.78[b]
O I	988.5, 988.6, 988.7, 1039, 1302	14.93 ± 0.05
Al II	1670	12.19 ± 0.06
Si II	989, 1193, 1260, 1304	13.75 ± 0.04
S II	1250	≤13.75[b]
Fe II	1608	13.33 ± 0.06

[a]Penprase et al. (2010).
[b]3σ limiting rest-frame equivalent width.

4.4 J1037+0139: DLA at $z_{abs} = 2.70487$

This QSO was also observed in service mode with UVES on 2010 February 12–14 and again on 2010 March 5. J1037+0139 was also one of the QSOs observed independently by Penprase et al. (2010). It is one of the faintest QSOs in our sample, requiring a total of 26075 s of integration to achieve an S/N∼40 at 5000 Å. The Lyα line falls on the edge of the blue detector, but this does not affect the accuracy of the H I column density since the blue wing of the damped Lyα line is still intact, and can be fit using the redshift derived from the well-defined narrow metal absorption lines. Moreover, we have access to Lyβ, which also exhibits damping wings (although not as strong as that of Lyα). We derive an H I column density of log[N(H I)/cm^{-2}] = 20.50 ± 0.08, which is consistent with estimates derived from the SDSS spectrum (log[N(H I)/cm^{-2}] = 20.45; Prochaska & Wolfe 2009), as well as that derived by Penprase et al. (2010) (log[N(H I)/cm^{-2}] = 20.40 ± 0.25). We present our Voigt profile fit to the Lyα line in the top panel of Fig. 4.

Again, the metal absorption is concentrated in a single component, in this case with a Doppler parameter of 5.9 km s^{-1}. The corresponding column densities for all of the available ions are listed in Table 7. For this system, both C II λ1036 and λ1334 are saturated and blended; however, we have a robust measure of

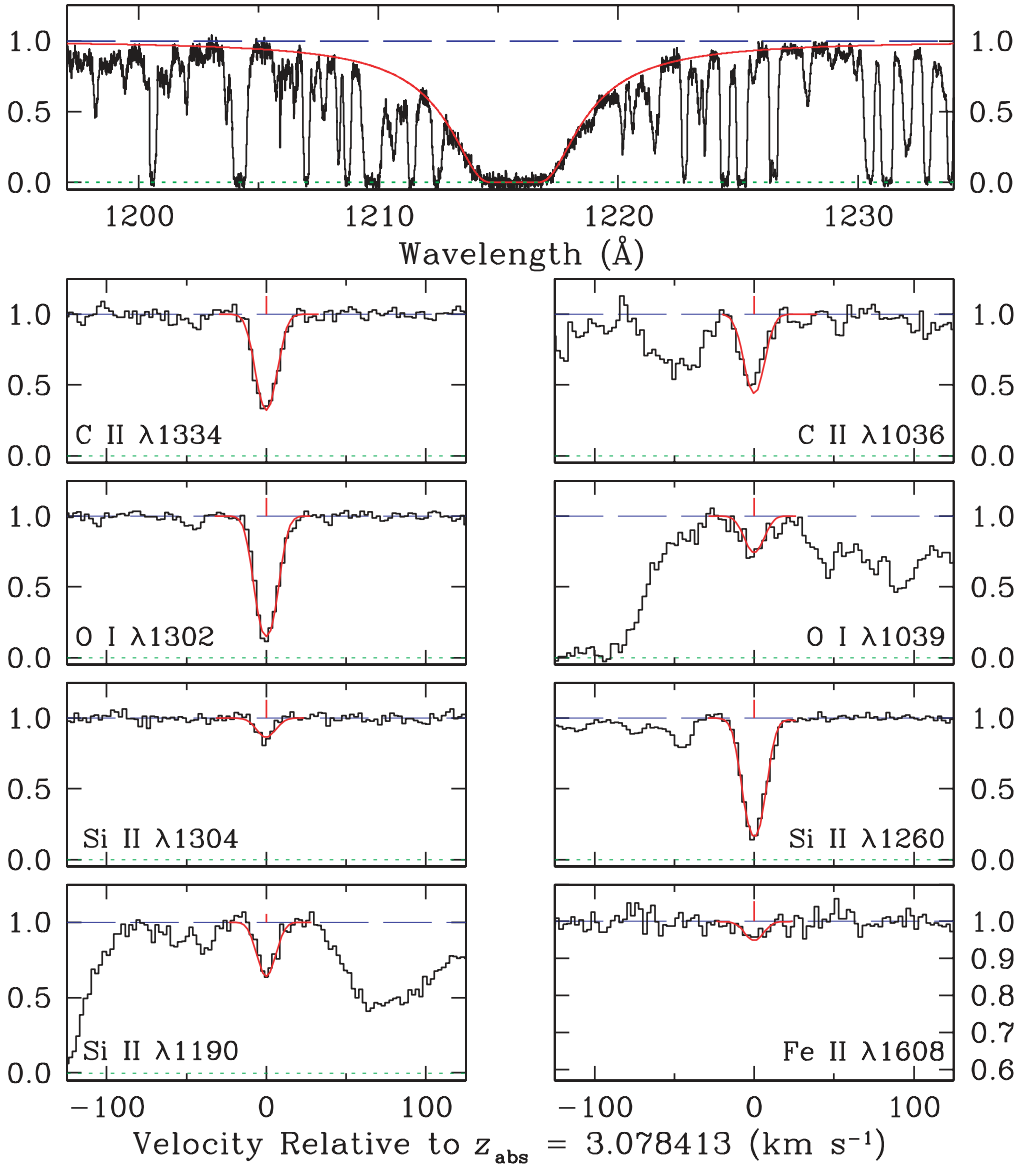

Figure 3. Same as Fig. 1, for the DLA towards J1001+0343 (black histogram) which exhibits a damped Lyα line at $z_{abs} = 3.07841$ (top panel). Here, the red continuous line shows the theoretical Voigt profile for an H I column density $\log[N(\mathrm{H\,I})/\mathrm{cm}^{-2}] = 20.21$. The remaining panels display a selection of metal lines. Note the different y-axis scale that is used for the weak Fe II λ1608 line (bottom-right panel).

Table 6. Ion column densities of the DLA in J1001+0343 at $z_{abs} = 3.07841$.

Ion	Transitions used	$\log N(\mathrm{X})/\mathrm{cm}^{-2}$
H I	1215	20.21 ± 0.05
C II	1036, 1334	13.58 ± 0.02
N I	1200.2	$\leq 12.50^a$
O I	1039, 1302	14.25 ± 0.02
Si II	1190, 1193, 1260, 1304, 1526	12.86 ± 0.01
S II	1253	$\leq 12.91^a$
Fe II	1608	12.50 ± 0.14

[a] 3σ limiting rest-frame equivalent width.

the O I and Fe II column densities from several unsaturated transitions. We also have a clear detection of the N I triplet near $\lambda_0 = 1200$ Å. Selected metal absorption lines are reproduced in Fig. 4.

4.5 J1340+1106: DLA at $z_{abs} = 2.50792$

This QSO has previously been observed with both UVES (at a spectral resolution of 10.3 km s^{-1} FWHM; Ledoux, Petitjean & Srianand 2003) and HIRES (at a spectral resolution of 8.1 km s^{-1} FWHM; Prochaska et al. 2003). However, given that this QSO intersects two VMP DLAs, one of which had potentially unsaturated C II lines, we decided to reobserve it with UVES for 29 800 s at a slightly higher spectral resolution of 7.3 km s^{-1}, and obtained complete spectral coverage from 3500 Å to almost 1 μm.

Since the broad damped profile of the Lyα line is independent of the spectral resolution, we combined the three data sets to obtain a high S/N near the damped Lyα line, from which we derived $\log[N(\mathrm{H\,I})/\mathrm{cm}^{-2}] = 20.09 \pm 0.05$. This model fit, along with the combined data, is shown in the top panel of Fig. 5. The profiles of the metal absorption lines, on the other hand, are narrow (FWHM $\lesssim$ 10 km s^{-1}); therefore, their observed profiles are not

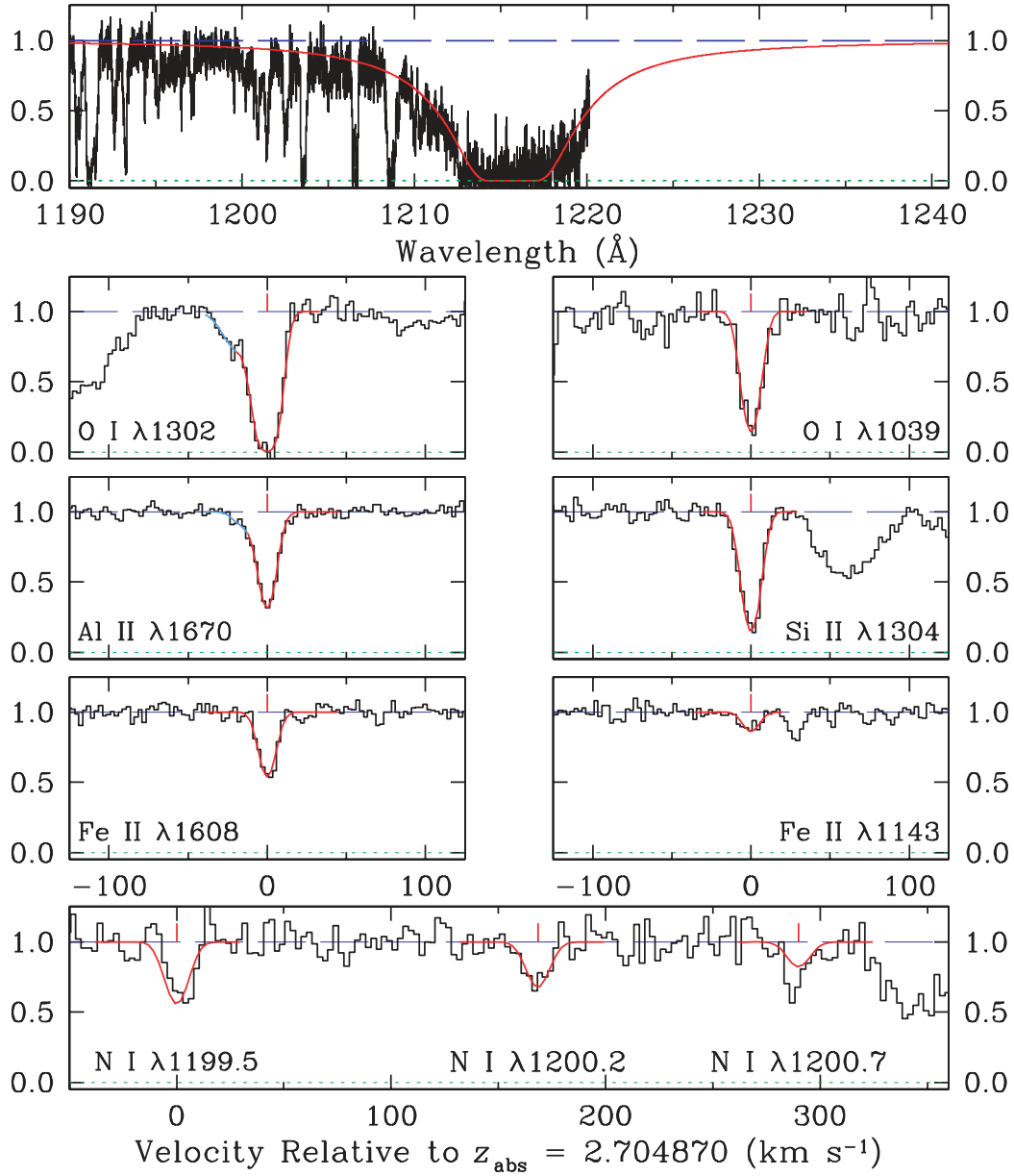

Figure 4. Same as Fig. 1, for the DLA towards J1037+0139 (black histogram) which exhibits a damped Lyα line at $z_{abs} = 2.70487$ (top panel). The red continuous line shows the theoretical Voigt profile for an H I column density $\log[N(\mathrm{H\,I})/\mathrm{cm}^{-2}] = 20.50$. The remaining panels display a selection of metal lines.

Table 7. Ion column densities of the DLA in J1037+0139 at $z_{abs} = 2.70487$.

Ion	Transitions used	$\log N(\mathrm{X})/\mathrm{cm}^{-2}$
H I	1025, 1215	20.50 ± 0.08
N I	1199.5, 1200.2, 1200.7	13.27 ± 0.04
O I	1039, 1302	15.06 ± 0.04
Al II	1670	12.32 ± 0.03
Si II	1260, 1304	13.97 ± 0.03
Fe II	1143, 1144, 1608	13.53 ± 0.02

independent of the spectral resolution. Thus, we separately combined the data of equal spectral resolution and individually read these three reduced spectra into VPFIT, which convolved the fitted model with the spectral resolution appropriate to the data. The upshot of proceeding in this way is that the cloud model is then largely driven by the data set of highest S/N for each absorption line that is input. However, since we cannot combine all three data sets, in Fig. 5 we only present the data set with the highest S/N near each absorption line.

Unfortunately, both of the C II absorption lines are saturated, and partially arise from nearby ionized gas, exhibiting a similar profile shape to the Al II λ1670 line. In fact, most of the metal absorption lines exhibit a second component on the blue wing (at $v = -23$ km s^{-1} relative to the main component at $z_{abs} = 2.507921$), which appears to arise from ionized gas. This is confirmed by the absence of this blue component in O I absorption (see O I λ1302, and note that the absorption on the blue wing of the O I λ1039 line is due to unrelated absorption), which has long been known to accurately trace neutral gas (Field & Steigman 1971). The presence of ionized

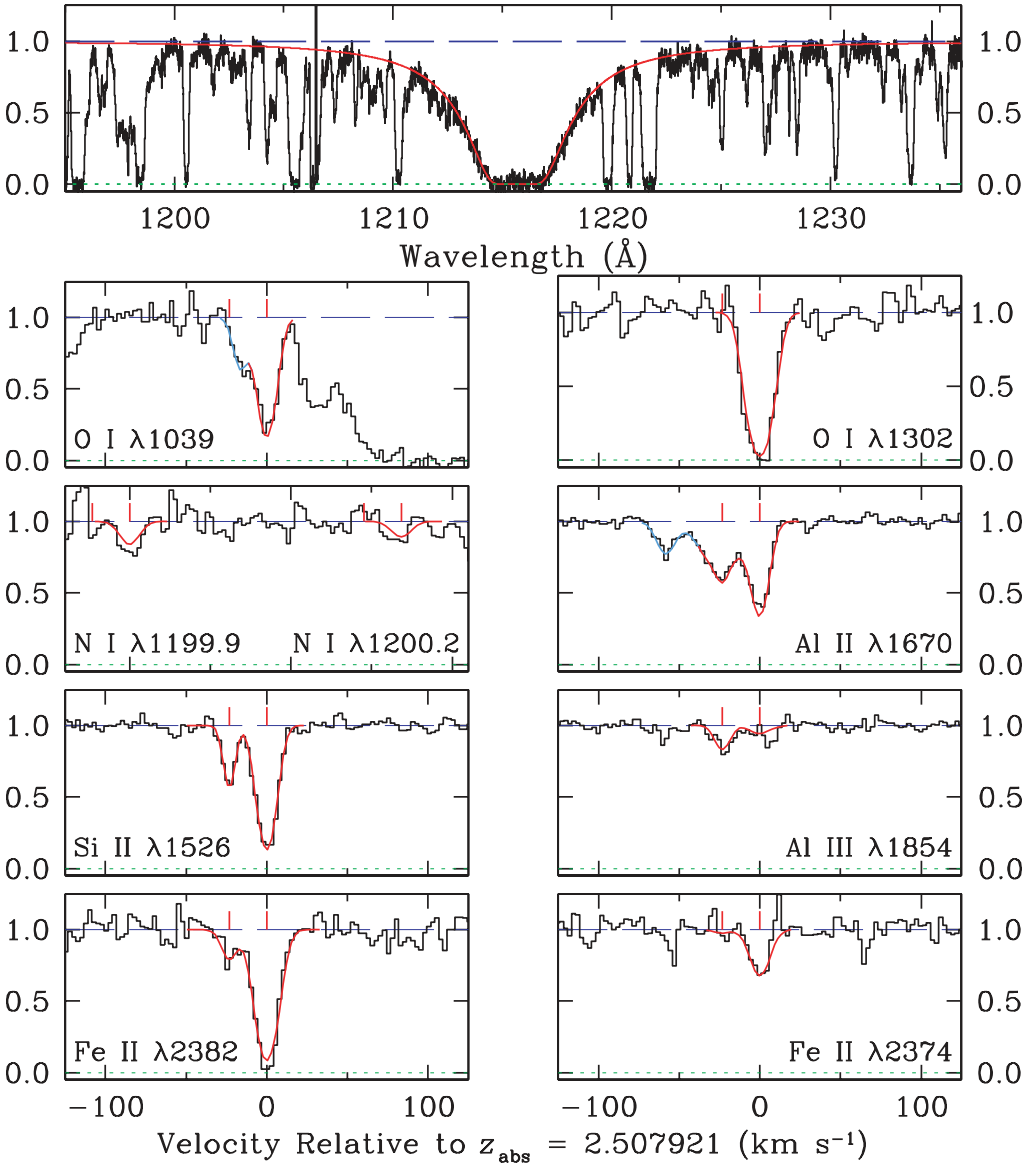

Figure 5. Same as Fig. 1, for the DLA towards J1340+1106 (black histogram) which exhibits a damped Lyα line at $z_{abs} = 2.50792$ (top panel). The red continuous line shows the theoretical Voigt profile for an H I column density $\log[N(\mathrm{H\,I})/\mathrm{cm}^{-2}] = 20.09$. The remaining panels display a selection of metal lines.

Table 8. Ion column densities of the DLA in J1340+1106 at $z_{abs} = 2.50792$.

Ion	Transitions used	$\log N(\mathrm{X})/\mathrm{cm}^{-2}$
H I	1215	20.09 ± 0.05
N I	1199.5, 1200.2	12.80 ± 0.04
O I	1039, 1302	15.02 ± 0.03
Al II	1670	12.27 ± 0.02
Al III	1854, 1862	11.51 ± 0.10
Si II	1190, 1193, 1304, 1526	13.75 ± 0.02
Fe II	1096, 1143, 2344, 2374, 2382	13.49 ± 0.02

gas is also confirmed by the higher Al III/Al II ratio exhibited by the blue component.

We derived the cloud model for both of these components from the host of available Si II and Fe II lines, with additional constraints coming from the two O I lines. In Table 2 we present the fitting results from both the blue component (component 1; which arises from nearby mildly ionized gas), and the main component (component 2) which we attribute to the DLA. Fixing the parameters of this cloud model, we then derived the column density for all ions in both components. In Table 8, however, we only provide the column density for the single, dominant component that we attribute to the DLA. The model fits to the data are presented in the lower panels of Fig. 5 where, as stated above, we only present the model and data that correspond to the highest S/N for each absorption line.

The detection of ions that arise in ionized gas, such as Al III, will later provide a useful means to test the accuracy of one of our underlying assumptions: that we can use the single dominant ion for each element to estimate the elemental abundances in DLAs (see Section 5.1).

4.6 J1340+1106: DLA at $z_{abs} = 2.79583$

We now report on the second VMP DLA that is intersected by this QSO. Again, we treat the Lyα line and the metal lines of this DLA as detailed in Section 4.5. From the combined data we derive an H I column density of $\log[N(\mathrm{H\,I})/\mathrm{cm}^{-2}] = 21.00 \pm 0.06$. The combined spectrum in the region of the damped Lyα line, together with the profile fit, is reproduced in the top panel of Fig. 6.

Turning now to the metal absorption lines, we have found that a two-component cloud model (with Doppler parameters of 9.2 ± 0.1 and $6.55 \pm 0.05\,\mathrm{km\,s^{-1}}$ separated by $22\,\mathrm{km\,s^{-1}}$) provides a good fit to the data. This cloud model is perhaps the best determined in our data set, given the high S/N of the data, and the numerous atomic transitions available. Our Voigt profile fits to the metal lines are shown in the lower panels of Fig. 6. However, as discussed in Section 4.5, we only present the model and data that correspond to the highest S/N for each absorption line. The column densities for all available ions are provided in Table 9. In this table, we have also provided the column densities for Al III and N II, which are coincident with the DLA, but are typically associated with H II regions.

4.7 J1419+0829: DLA at $z_{abs} = 3.04973$

We recorded the spectrum of J1419+0829 ($z_{em} = 3.034$) for 29 800 s with UVES in service mode, resulting in an S/N near 5000Å (near the red wing of the damped Lyα line) of $\simeq$40. This high S/N in combination with a virtually uninterrupted red wing to the Lyα absorption allows a very accurate measurement of the H I column density, $\log[N(\mathrm{H\,I})/\mathrm{cm}^{-2}] = 20.40 \pm 0.03$. The Voigt profile fit to the Lyα line is shown in the top panel of Fig. 7, with a

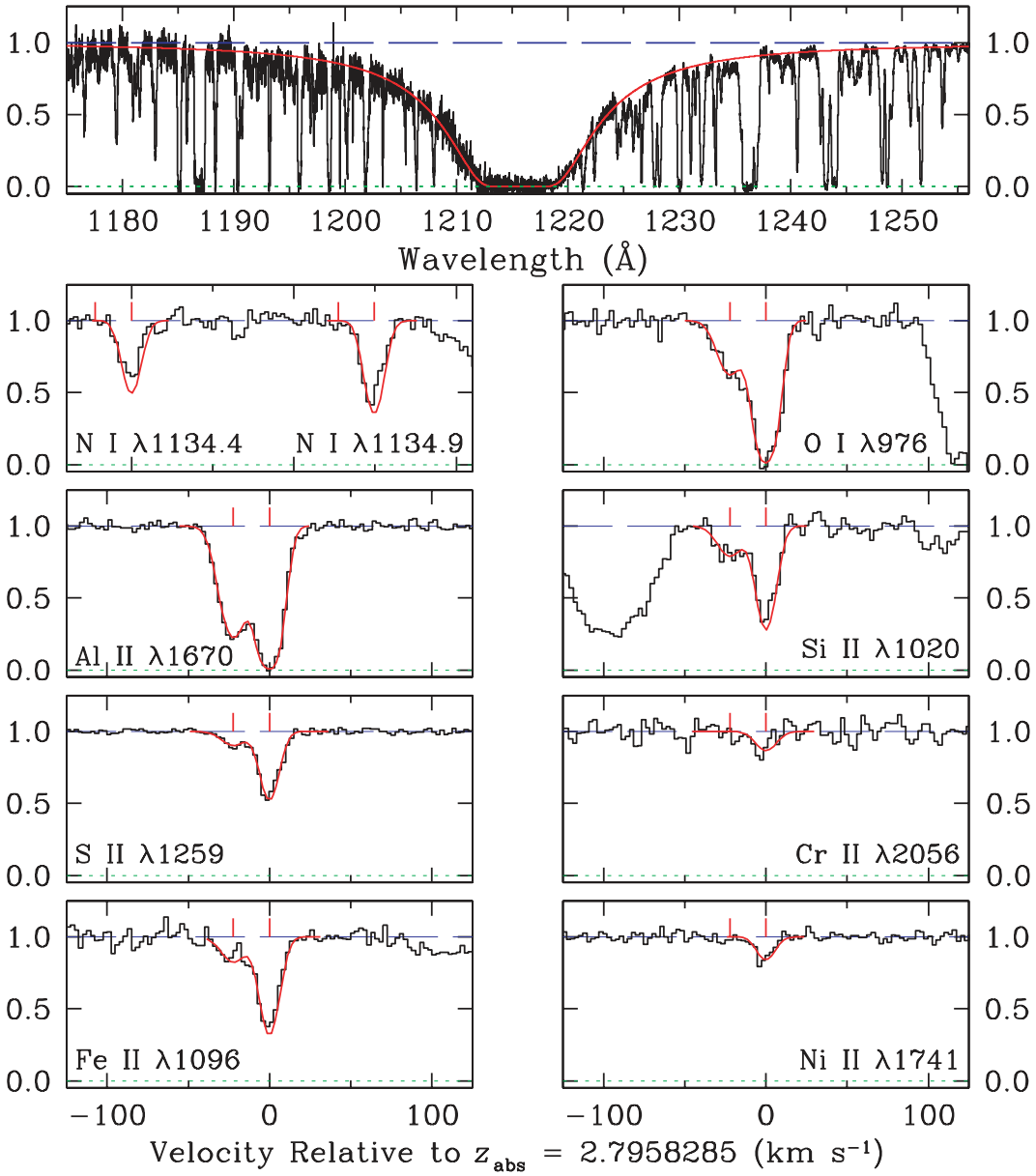

Figure 6. Same as Fig. 1, for the DLA towards J1340+1106 (black histogram) which exhibits a damped Lyα line at $z_{abs} = 2.79583$ (top panel). The red continuous line shows the theoretical Voigt profile for an H I column density $\log[N(\mathrm{H\,I})/\mathrm{cm}^{-2}] = 21.00$. The remaining panels display a selection of metal lines.

Table 9. Ion column densities of the DLA in J1340+1106 at $z_{abs} = 2.79583$.

Ion	Transitions used	$\log N(\mathrm{X})/\mathrm{cm}^{-2}$
H I	1215	21.00 ± 0.06
C II*	1335	12.99 ± 0.04
N I	1134.4, 1134.9, 1199.5, 1200.7	14.04 ± 0.02
N II	1083	12.81 ± 0.09
O I	925, 976, 1302	16.04 ± 0.04
Al II	1670	13.24 ± 0.03
Al III	1854, 1862	12.19 ± 0.08
Si II	1020, 1193, 1260, 1304, 1526, 1808	14.68 ± 0.02
S II	1253, 1259	14.30 ± 0.02
Ar I	1048, 1066	13.18 ± 0.02
Cr II	2056, 2062	12.62 ± 0.11
Fe II	1063.1, 1081, 1096, 1125, 1608, 1611, 2260, 2344, 2382	14.32 ± 0.01
Ni II	1317, 1370, 1454, 1709, 1741, 1751	13.08 ± 0.03

selection of the associated metal absorption lines in the remaining panels.

A cloud model with two components separated by $\sim$14 km s^{-1} (Table 2) provides a good fit to the data. This cloud model is well determined by a host of O I and Si II lines (see Table 10). Both C II λ1334 and λ1036 are saturated; column densities for N I, O I, Si II and Fe II are listed in Table 10.

4.8 The final VMP DLA sample

In order to augment our survey of VMP DLAs, we have searched the literature for known examples satisfying the following conditions: (i) the QSO spectra were observed at high spectral resolution ($R > 30\,000$) – in practice this meant that the data were recorded with either UVES or HIRES; (ii) [Fe/H] ≤ -2.0; and (iii) at least one unsaturated O I absorption from which [O/H] could be measured. These conditions were imposed to select a sample of measurements from the literature which is highly compatible to our own data and whose metal abundances could be adopted without reanalysing the spectra (although we referred all measurements to the same solar abundance scale – see Section 5). The literature trawl yielded an additional 10 DLAs satisfying the above conditions; together with our own observations they form a sample of 22 VMP DLAs. The metallicity distribution function for this sample, which appears to tail off towards the lowest metallicities, is shown in Fig. 8.

Relevant details of the full sample are collected in Table 11, where we list absorption redshifts, neutral hydrogen column densities and element abundances for a selection of the metals most commonly observed in VMP DLAs, including: (1) C, N, O – the first elements synthesized in the chain of stellar nucleosynthesis; (2) Al – an odd atomic number element; (3) Si – an even atomic number element and (4) Fe – an iron-peak element. The uncertainty in each abundance includes the error in H I. In Appendix A, we provide a similar table listing the column densities of each ion from which these abundances were derived.

5 ABUNDANCE ANALYSIS

As in previous DLA work, we assume that each element resides in a single dominant ionization stage in the neutral gas. Thus, the abundance of a given element is found by taking the ratio of the dominant ions column density to that of H I, and referring it to a solar scale [i.e. $[\mathrm{X/H}] = \log(N(\mathrm{X})/N(\mathrm{H\,I})) - \log(\mathrm{X/H})_{\odot}$]. Throughout this article, we adopt the Asplund et al. (2009) solar scale, taking the photospheric, meteoritic or the average of the two, based on the suggestion by Lodders, Plame & Gail (2009). The adopted abundances relevant to this work are collected in Table 12.

Thus, measuring elemental abundances in VMP DLAs is a relatively straightforward process. Some uncertainty arises, however, if the observed metal-line absorption from ions that are dominant in H I regions does not perfectly trace the H I gas. For example, if the dominant ion for a given element is also present in nearby H II gas (often the case for singly ionized species; e.g. C II, Si II, Fe II), we will overestimate the abundance of this element. On the other hand, if the dominant ion for a given element is mildly ionized in the H I gas itself (usually the case for neutral species; e.g. N I), we will underestimate the element's abundance. In addition to these ionization corrections, further uncertainties may be introduced into the abundance analysis if some refractory elements have condensed to form dust grains. Whilst both of these concerns are expected to be negligible in the VMP regime (Vladilo et al. 2001; Vladilo 2004), we reassess their importance in the following subsections.

5.1 Ionization corrections

Ionization corrections are known to be small when the neutral hydrogen column density is in excess of $\sim 10^{20}$ atoms cm^{-2}. Nevertheless, for each element X with the dominant ionization stage N, one needs to apply a small correction, IC(X), to recover the *true* elemental abundance,

$$[\mathrm{X/H}] = [\mathrm{X\,N/H\,I}] + \mathrm{IC(X)}. \quad (1)$$

To estimate the magnitude of such corrections, we used the CLOUDY photoionization software developed by Ferland et al. (1998) to model two of the VMP DLAs from our sample, chosen to represent the range of N(H I) values that we report: one DLA with a low H I column density (the DLA with $\log[N(\mathrm{H\,I})/\mathrm{cm}^{-2}] = 20.09$ towards J1340+1106 at $z_{abs} = 2.50792$) and the other with a high N(H I) (the DLA with $\log[N(\mathrm{H\,I})/\mathrm{cm}^{-2}] = 21.00$ towards J1340+1106 at $z_{abs} = 2.79583$). In both cases, we modelled the VMP DLA as a plane-parallel slab of constant volume density gas in the range $-3 < \log[n(\mathrm{H})/\mathrm{cm}^{-3}] < 3$, irradiated by the cosmic microwave background and UV background (Haardt & Madau 2001) at the appropriate redshift. Using the solar abundance scale in Table 12 we globally scaled the metal abundances of the VMP DLA to be 10^{-2} Z$_{\odot}$. The simulations were stopped once the H I column density of the DLA was reached, at which point we output the simulated ion column densities of the slab.

Once the above value of the background radiation field is assumed, the ionization correction for each element depends on the volume density of the gas (left-hand panels of Fig. 9), which may be estimated by considering the ratio of successive ion stages (right-hand panels of Fig. 9). For the low N(H I) DLA being considered as an example here, we measure $N(\mathrm{Al\,III})/N(\mathrm{Al\,II}) = -0.76 \pm 0.10$, implying a gas density of $\log[n(\mathrm{H})/\mathrm{cm}^{-3}] \simeq -1.2 \pm 0.4$. For the high N(H I) DLA, we measure $N(\mathrm{Al\,III})/N(\mathrm{Al\,II}) = -1.05 \pm 0.09$ and $N(\mathrm{N\,II})/N(\mathrm{N\,I}) = -1.23 \pm 0.09$, which are both consistent with a gas density of $\log[n(\mathrm{H})/\mathrm{cm}^{-3}] \simeq -1.1 \pm 0.2$. At these values of the gas density, it can be seen that the ionization corrections for the VMP DLAs in our sample are $\lesssim$0.1 dex for the main elements of interest.

We also performed the above calculations under the assumption of a softer background radiation field (i.e. an O star) rather than the Haardt & Madau (2001) background. Our results are quantitatively similar to those of Vladilo et al. (2001): corrections for all of the

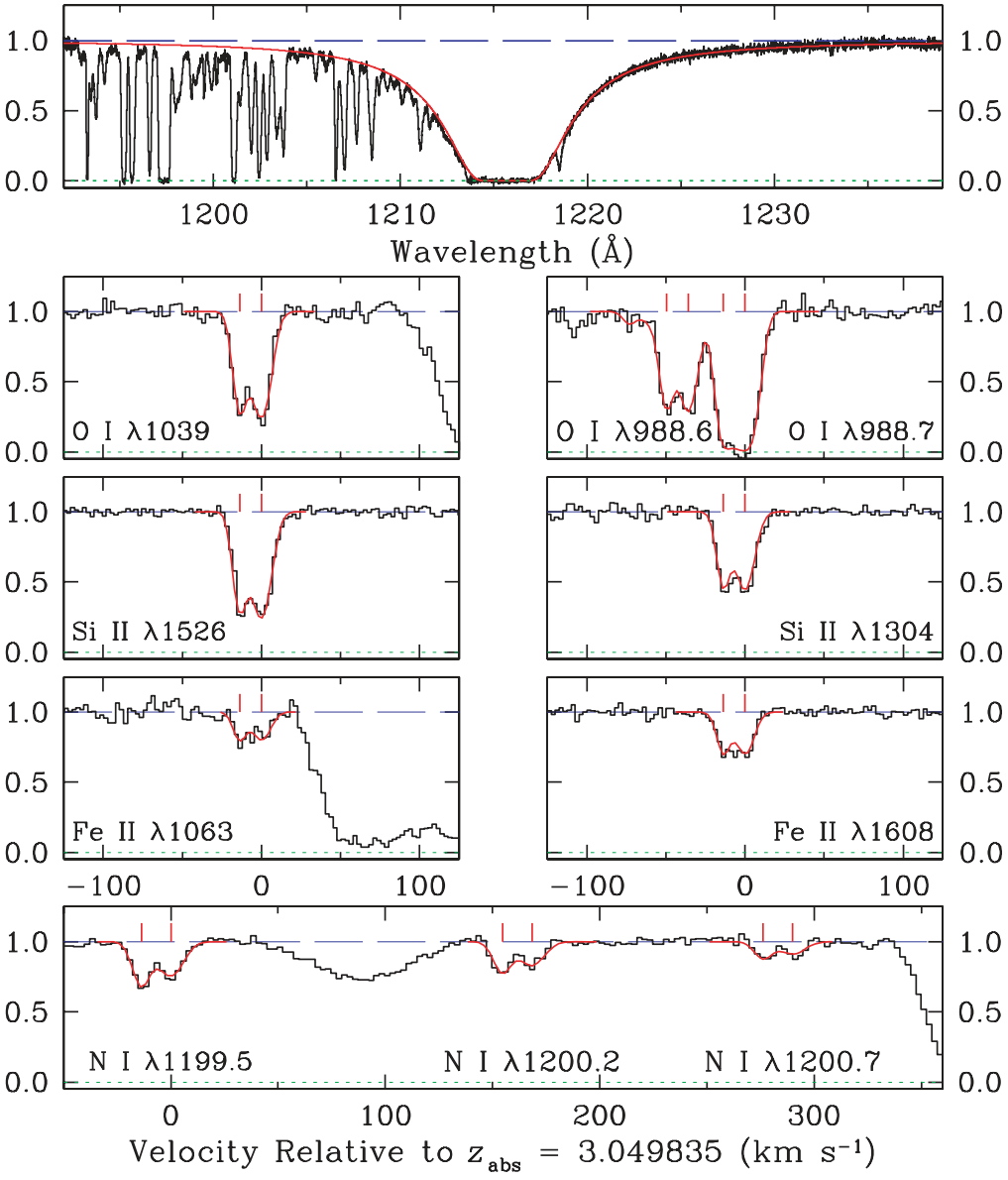

Figure 7. Same as Fig. 1, for the DLA towards J1419+0829 (black histogram) which exhibits a damped Lyα line at $z_{abs} = 3.04973$ (top panel). The red continuous line shows the theoretical Voigt profile for an H I column density $\log[N(\mathrm{H\,I})/\mathrm{cm}^{-2}] = 20.40$. The remaining panels display a selection of metal lines.

Table 10. Ion column densities of the DLA in J1419+0829 at $z_{abs} = 3.04973$.

Ion	Transitions used	$\log N(\mathrm{X})/\mathrm{cm}^{-2}$
H I	1025, 1215	20.40 ± 0.03
N I	1199.5, 1200.2, 1200.7	13.28 ± 0.02
O I	936, 948, 976, 988.5, 988.6, 988.7, 1039, 1302	15.17 ± 0.02
Si II	989, 1190, 1193, 1260, 1304, 1526	13.83 ± 0.01
Fe II	1063.1, 1608	13.54 ± 0.03

elements we are interested in are $\lesssim$0.1 dex, except for Al II which can require corrections of the order $\sim$0.3 dex for the lowest column density systems. At present, it is not yet clear whether these VMP systems harbour (or nearby to) stellar populations such as massive Population II or Population III stars. Based on the results described in this section, we have therefore not corrected any of the measured abundances for ionization effects.

5.2 Dust depletion

To measure accurately element abundances in DLAs, the fraction of a given element that is not observed in the gas phase, but is instead locked up in dust grains, must also be considered. To account for this effect, one ideally considers the relative abundances of a refractory and a volatile element (e.g. [Cr/Zn]), and compares this to the expected intrinsic nucleosynthetic ratio (typically the ratio seen in stars of comparable metallicity). Previous studies based on such a comparison have shown that DLAs exhibit minimal dust depletion when [Fe/H] $\lesssim -2.0$ (Pettini et al. 1997; Akerman et al. 2005). Unfortunately, the Cr II and Zn II lines are too weak in the VMP regime to be measured, so one needs to resort to more abundant elements, such as Si and Fe, which are known to be depleted to different degrees (Fe is more readily incorporated into dust grains than Si).

The most metal-poor stars in the halo of our Galaxy suggest that the intrinsic nucleosynthetic ratio of Si/Fe is virtually

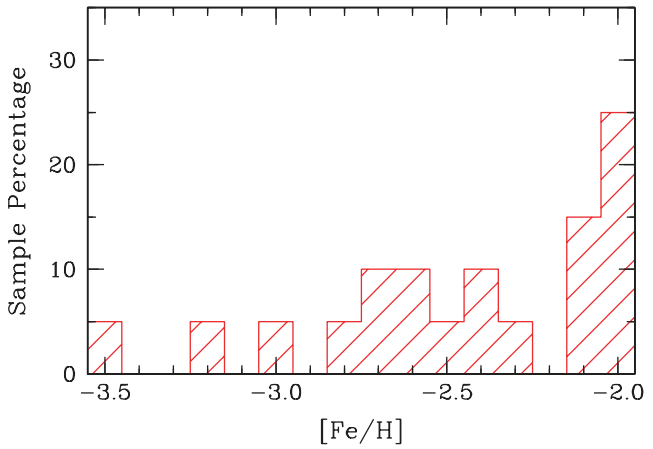

Figure 8. The metallicity distribution function for the sample of VMP DLAs listed in Table 11 is shown as the red histogram.

independent of metallicity, corresponding roughly to a constant of [Si/Fe] = +0.37 ± 0.15 (Cayrel et al. 2004). Such a plateau was first seen in DLAs by Prochaska & Wolfe (2002), who found [Si/Fe] ≃ +0.3 when [Fe/H] < −2 (see updated version in Wolfe et al. 2005). A similar study was also conducted by Vladilo (2002), who suggested there may still exist some mild depletion on to dust, resulting in a plateau of [Si/Fe] ≃ +0.25. From the 19 VMP DLAs in our sample, we find that [⟨Si/Fe⟩] = +0.32 ± 0.09, which is certainly consistent with minimal dust depletion. We therefore proceed under the assumption that dust has a negligible effect on our derived elemental abundances.

6 COMPARING VMP DLAS AND STARS

DLAs likely experience very different chemical histories to that of the stars in the halo of our Galaxy. However, in the limit of decreasing metallicity, both stars and DLAs are polluted by very few previous generations of stars. In fact, since the physical conditions of the gas that gives rise to DLAs are conducive to forming stars (Noterdaeme et al. 2008; Jorgenson et al. 2009), it certainly seems plausible that some of the VMP stars in the halo of our Galaxy originally condensed out of a VMP DLA. If this is indeed true, we would therefore expect both VMP stars and DLAs to share similar chemical signatures at the lowest metallicities. In the following sections, we test the validity of this expectation by directly comparing the abundances of the VMP DLAs in this survey to the most recent abundance measurements of VMP stars.

6.1 Revisiting C/O at low metallicity

We first consider the trend of C/O at low metallicity, which has received a great deal of attention in recent years. The evolution of the C/O ratio when [O/H] $\gtrsim -1.0$ has been known for a while; [C/O] increases linearly from ~ -0.6 to solar with increasing [O/H] (see Fig. 10). This trend is thought to be due to the increased, metallicity-dependent, carbon yields of massive rotating stars, combined with

Table 11. C, N, O, Al, Si and Fe abundance measurements in VMP DLAs.

QSO	z_{abs}	$\log N(\mathrm{H\,I})$ ($\mathrm{cm^{-2}}$)	[C/H]	[N/H]	[O/H]	[Al/H]	[Si/H]	[Fe/H]	Ref.[a]
Our VMP DLA sample									
J0035−0918	2.34010	20.55 ± 0.10	−1.51 ± 0.18	−2.87 ± 0.12	−2.28 ± 0.13	−3.26 ± 0.11	−2.65 ± 0.11	−3.04 ± 0.12	2
J0311−1722	3.73400	20.30 ± 0.06	−2.71 ± 0.10	≤−3.06	−2.29 ± 0.10	...	−2.50 ± 0.09	≤−2.01	1
J0831+3358	2.30364	20.25 ± 0.15	...	≤−3.30	−2.01 ± 0.16	−2.50 ± 0.16	−2.01 ± 0.16	−2.39 ± 0.16	1,4
Q0913+072	2.61843	20.34 ± 0.04	−2.79 ± 0.06	−3.88 ± 0.13	−2.40 ± 0.04	−3.00 ± 0.05	−2.55 ± 0.04	−2.82 ± 0.04	3
J1001+0343	3.07841	20.21 ± 0.05	−3.06 ± 0.05	≤−3.54	−2.65 ± 0.05	...	−2.86 ± 0.05	−3.18 ± 0.15	1
J1016+4040	2.81633	19.90 ± 0.11	−2.67 ± 0.12	≤−2.97	−2.46 ± 0.11	...	−2.51 ± 0.12	...	3
J1037+0139	2.70487	20.50 ± 0.08	...	−3.06 ± 0.09	−2.13 ± 0.09	−2.62 ± 0.09	−2.04 ± 0.09	−2.44 ± 0.08	1
J1340+1106	2.50792	20.09 ± 0.05	...	−3.12 ± 0.06	−1.76 ± 0.06	−2.26 ± 0.05	−1.85 ± 0.05	−2.07 ± 0.05	1
J1340+1106	2.79583	21.00 ± 0.06	...	−2.79 ± 0.06	−1.65 ± 0.07	−2.20 ± 0.07	−1.83 ± 0.06	−2.15 ± 0.06	1
J1419+0829	3.04973	20.40 ± 0.03	...	−2.95 ± 0.04	−1.92 ± 0.04	...	−2.08 ± 0.03	−2.33 ± 0.04	1
J1558+4053	2.55332	20.30 ± 0.04	−2.51 ± 0.07	−3.47 ± 0.08	−2.45 ± 0.06	−2.82 ± 0.07	−2.49 ± 0.04	−2.70 ± 0.07	3
Q2206−199	2.07624	20.43 ± 0.04	−2.45 ± 0.05	−3.47 ± 0.06	−2.07 ± 0.05	−2.69 ± 0.04	−2.29 ± 0.04	−2.57 ± 0.04	3
Literature VMP DLAs									
Q0000−2620	3.39012	21.41 ± 0.08	...	−2.54 ± 0.08	−1.68 ± 0.13	...	−1.86 ± 0.08	−2.01 ± 0.09	5
Q0112−306	2.41844	20.50 ± 0.08	...	−3.17 ± 0.09	−2.24 ± 0.11	...	−2.39 ± 0.08	−2.64 ± 0.09	6
J0140−0839	3.69660	20.75 ± 0.15	−3.05 ± 0.17	≤−4.20	−2.75 ± 0.15	−3.37 ± 0.16	−2.75 ± 0.17	−3.45 ± 0.24[b]	7
J0307−4945	4.46658	20.67 ± 0.09	...	−2.93 ± 0.15	−1.45 ± 0.19	−1.75 ± 0.11	−1.50 ± 0.11	−1.93 ± 0.19	8
Q1108−077	3.60767	20.37 ± 0.07	...	≤−3.36	−1.69 ± 0.08	...	−1.54 ± 0.07	−1.96 ± 0.07	6
J1337+3153	3.16768	20.41 ± 0.15	−2.86 ± 0.16	≤−3.44	−2.67 ± 0.17	−2.85 ± 0.16	−2.68 ± 0.16	−2.74 ± 0.30	9
J1558−0031	2.70262	20.67 ± 0.05	...	−2.04 ± 0.05[c]	−1.50 ± 0.05[c]	...	−1.94 ± 0.05[c]	−2.03 ± 0.05[c]	10
Q1946+7658	2.84430	20.27 ± 0.06	...	−3.51 ± 0.07	−2.14 ± 0.06	...	−2.18 ± 0.06	−2.50 ± 0.06	11
Q2059−360	3.08293	20.98 ± 0.08	...	−2.86 ± 0.08	−1.58 ± 0.09	...	−1.63 ± 0.09	−1.97 ± 0.08	6
J2155+1358	4.21244	19.61 ± 0.10	−2.09 ± 0.12	...	−1.80 ± 0.11	−2.13 ± 0.20	−1.87 ± 0.11	−2.15 ± 0.25	12

[a]References – 1: This work; 2: Cooke et al. (2011); 3: Pettini et al. (2008); 4: Penprase et al. (2010); 5: Molaro et al. (2000); 6: Petitjean, Ledoux & Srianand (2008); 7: Ellison et al. (2010); 8: Dessauges-Zavadsky et al. (2001); 9: Srianand et al. (2010); 10: O'Meara et al. (2006); 11: Prochaska et al. (2002); 12: Dessauges-Zavadsky et al. (2003).

[b]Ellison et al. (2010) quote a 3σ upper limit to the Fe II column density of $\log N(\mathrm{Fe\,II})/\mathrm{cm^{-2}} < 12.73$. We have since rereduced these data (as described in Section 2), and detected the Fe II λ1608 line at the 4σ level. The Fe abundance quoted here is derived using the optically thin limit approximation to measure N(Fe II).

[c]The metal ion uncertainty for this measurement was not provided by the authors. Thus, we only quote the uncertainty in N(H I).

Table 12. Adopted solar abundances.

X	$\log(X/H)_\odot$	X	$\log(X/H)_\odot$
C	−3.57	S	−4.86
N	−4.17	Ar	−5.60
O	−3.31	Cr	−6.36
Al	−5.56	Fe	−4.53
Si	−4.49	Ni	−5.79

the delayed release of carbon from low- and intermediate-mass stars (Akerman et al. 2004). Based on current models of Population II nucleosynthesis, below [O/H] ~ -1.0, [C/O] is predicted to decrease (or perhaps plateau) with decreasing metallicity. Indeed, such a plateau was first reported for a sample of halo stars by Tomkin et al. (1992), who measured [C/O] abundances down to [O/H] ~ -1.7.

This work was extended to even lower oxygen abundances by Akerman et al. (2004) and Spite et al. (2005). Contrary to the supposed decrease in [C/O], these authors uncovered quite the opposite trend when [O/H] $\lesssim -2.0$; an extrapolation of this trend suggests that [C/O] could reach near-solar values when [O/H] ~ -3.0. Three possibilities have been suggested to explain this behaviour: (1) the leftover signature of a high-carbon producing generation of Population III stars (Chieffi & Limongi 2002; Umeda & Nomoto 2003; Heger & Woosley 2010); (2) pollution from a previous generation of rapidly rotating low-metallicity Population II stars (Chiappini et al. 2006); or (3) systematic uncertainties in the adopted 1D LTE analysis. The third of these possibilities has recently been ruled out by Fabbian et al. (2009a), who conducted a more detailed analysis of the lines used by Akerman et al. (2004), thus confirming the stellar C/O trend at low metallicity.

Such an 'unexpected' trend is perhaps not so surprising in hindsight, since several other lines of evidence support a high-carbon producing generation of early stars, including: (1) the fact that a high carbon abundance is *required* at early times to efficiently cool the gas, and drive the transition from Population III to Population II star formation (Frebel, Johnson & Bromm 2007); (2) observations of the three most iron-poor stars known to date have revealed that they all exhibit extreme carbon enhancements (Christlieb et al. 2002; Frebel et al. 2005; Norris et al. 2007); (3) in addition, the fraction of all carbon-enhanced metal-poor (CEMP) stars is thought to increase with decreasing metallicity (Beers & Christlieb 2005); (4) for at least a subset of these CEMP stars, it has been suggested that their carbon-enhancement reflects the composition of the cloud of gas from which the CEMP star first condensed (Ryan et al. 2005; Aoki et al. 2007); and (5) the observed fraction of CEMP stars in the outer halo component of our Galaxy is roughly twice that of the inner halo component, which favours the existence of a high carbon-producing source other than asymptotic giant branch stars (Carollo et al. 2011).

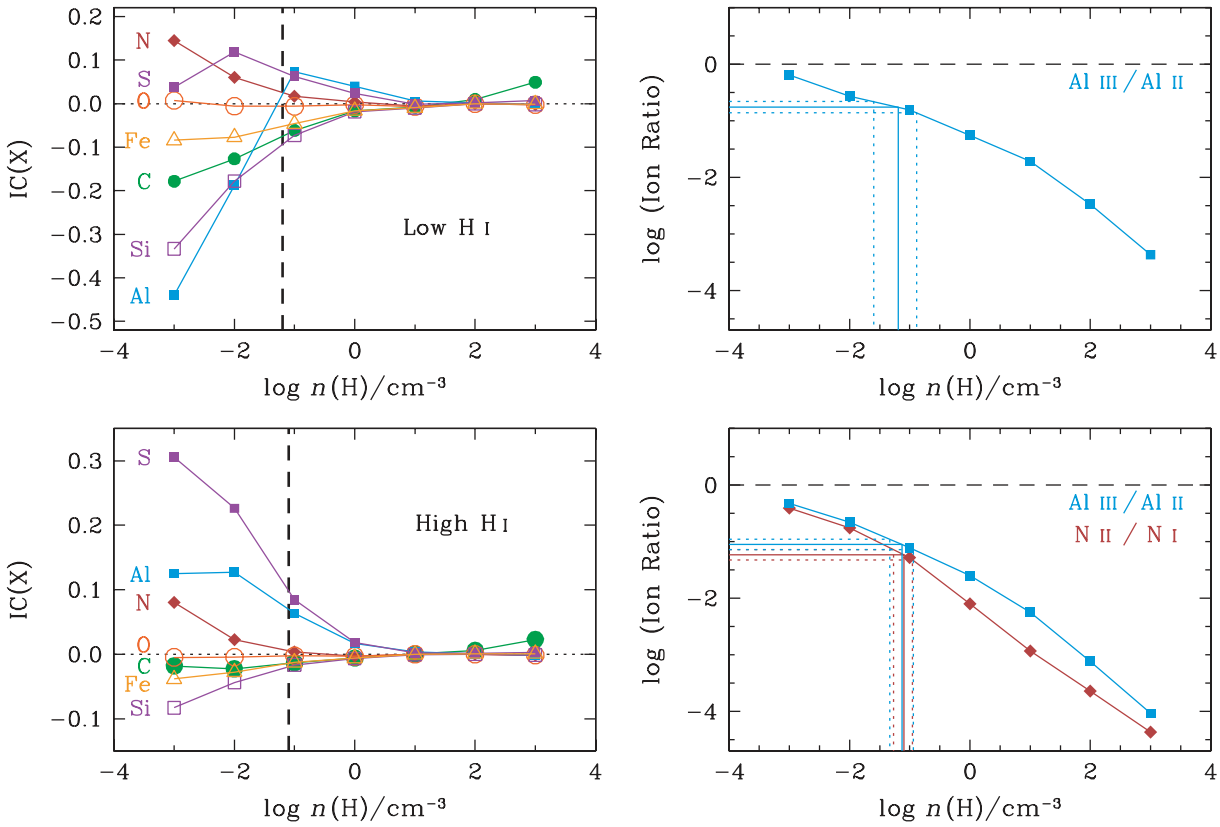

Figure 9. Ionization corrections for two typical VMP DLAs, respectively with low and high H I column density. Left-hand panels: the ionization corrections, as defined by equation (1), for the most commonly observed elements in VMP DLAs are plotted as a function of gas volume density. The vertical dashed lines correspond to the estimated gas densities of the two DLAs (shown by the solid vertical line in the right-hand panels). Right-hand panels: column density ratios for successive ion stages of Al (blue squares connected by a solid line) and N (red diamonds connected by a solid line) versus gas density. We also plot the observed values of the Al III/Al II and N II/N I ratios (solid horizontal lines) along with their uncertainties (dotted lines) for the two VMP DLAs we use as examples in this test (see text for further details).

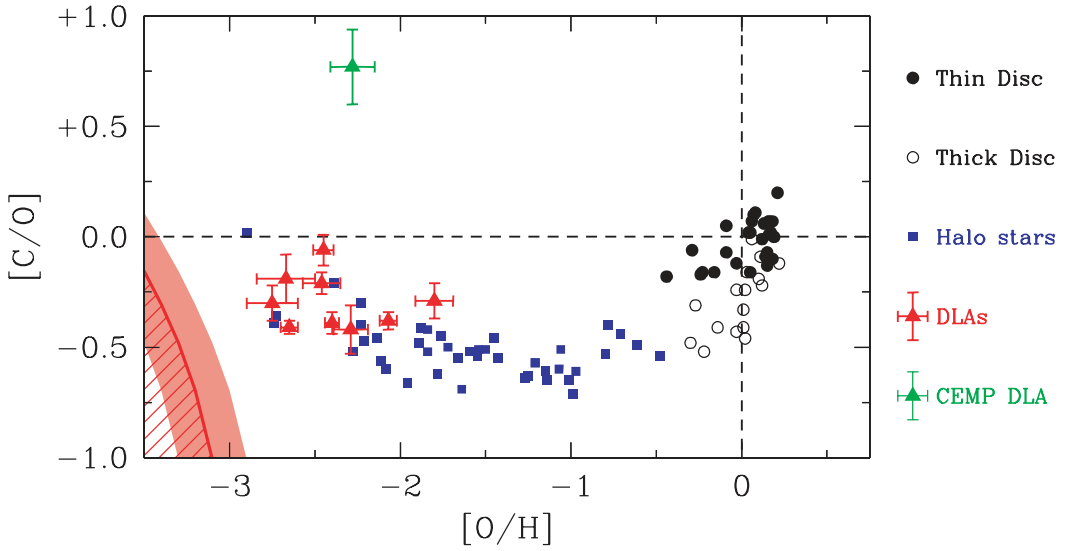

Figure 10. C and O abundances in VMP DLAs (red triangles) observed at high spectral resolution. The green triangle represents the carbon-enhanced DLA reported by Cooke et al. (2011). For comparison, we also plot the sample of metal-poor halo stars analysed by Fabbian et al. (2009a), where we adopt the values for C and O that are calculated assuming the Drawin (1969) formula for collisions with hydrogen ($S_{\rm H} = 1$; blue squares). We also show a sample of thin- and thick-disc stars (filled and open circles, respectively) from Bensby & Feltzing (2006). The red hatched region corresponds to the transition discriminant outlined by Frebel et al. (2007), where the uncertainty in this relation is shown by the light red shaded region. All abundances are relative to the Asplund et al. (2009) solar abundance scale (see Section 5).

Additional evidence for a high carbon-producing early generation of stars has recently been provided by studies of the most metal-poor DLAs (Pettini et al. 2008; Penprase et al. 2010), which probe entire clouds of near-pristine gas. Such surveys find that DLAs and stars tell the same story in the metal-poor regime – both show elevated, near-solar values of [C/O] when [O/H] $\lesssim -2.0$. In fact, the recent medium spectral resolution study by Penprase et al. (2010) suggests that [C/O] might further increase to *super-solar* values at even lower metallicity, although this still remains uncertain due to saturation effects. Further evidence for an increased carbon yield by an early generation of stars has recently come to light with the discovery by Cooke et al. (2011) of a metal-poor DLA which exhibits a C/Fe ratio 35 times greater than solar.

In Fig. 10, we show the updated plot of [C/O] versus [O/H] for our full DLA survey, together with values for the metal-poor halo stars (blue squares) analysed by Fabbian et al. (2009a),[9] and a sample of thin- and thick-disc stars with C and O abundances determined from forbidden lines (filled and open black circles, respectively; Bensby & Feltzing 2006). All data have been corrected for the updated Asplund et al. (2009) solar abundance scale (see Section 5). We first note that there is generally a good agreement – both in the trend and in the dispersion of [C/O] – between the most metal-poor stars and DLAs. The new DLA measurements reported here confirm the initial indications from the more limited samples considered by Pettini et al. (2008) and Penprase et al. (2010). The main departure from this trend is the CEMP DLA reported by Cooke et al. (2011), represented by the green triangle in Fig. 10. Aside from this system, no other DLA exhibits super-solar [C/O]. This statement is also true for the sample of seven O I absorbers at $z_{\rm abs} \sim 6$ recently reported by Becker et al. (2011, see also Becker et al. 2006).

[9] The data shown in Fig. 10 refer to cross-sections for collisions with hydrogen atoms based on the classical recipe of Drawin (1969), i.e. using a scaling factor $S_{\rm H} = 1$. If hydrogen collisions are completely neglected ($S_{\rm H} = 0$), this trend is 'stretched' to higher [C/O] (by about 0.2 dex) and lower [O/H] (by about 0.3 dex) at the lowest values of [O/H].

It is thus somewhat surprising that Penprase et al. (2010) found [C/O] ≥ 0.0 for four out of the five VMP DLAs in which they could measure this ratio. The difference may be due to different sample criteria between our survey and theirs: while we have excluded from our analysis absorption systems where the C II lines are saturated, such cases may be more difficult to recognize at the lower resolution of the ESI spectra analysed by Penprase et al. (2010). VMP DLAs with super-solar C/O ratios may well exist [and indeed the CEMP DLA discovered by Cooke et al. (2011) is one such example], but their C abundance is generally more difficult to measure with confidence due to line saturation. On the other hand, our survey is not biased against uncovering systems with *lower* [C/O] values than those reported here; thus, the VMP DLAs in our current sample define a *lower-envelope* in the [C/O] versus [O/H] plane. This envelope appears to be in good agreement with the envelope defined by VMP stars (see Fig. 10).

In Fig. 10 we also show the 'Frebel criterion' (red hatched region; Frebel et al. 2007; see also Bromm & Loeb 2003) which states that, if the fine-structure lines of O I and C II dominate the cooling in a near-pristine cloud of gas that has been enriched to some critical metallicity, then the first low-mass Population II stars will form. Thus, given these conditions, no Population II star should be observed in this red hatched region (where the uncertainty in this region is given by the light red shaded band). DLAs, on the other hand, are not restricted by this criterion. Indeed, if a cloud of gas was to be observed in this Population II star 'forbidden zone', it may very well form a collection of massive stars below or near the critical metallicity! Such systems, if found, would provide a unique window to study the transition from Population III to Population II star formation.

With these considerations in mind, we note that all DLAs in our sample will, perhaps unsurprisingly, form Population II stars. One might, therefore, be tempted to conclude that the stars in the halo of our Milky Way represent the same distribution that defines VMP DLAs. To test this possibility, we performed a linear fit to [C/O] versus [O/H] for the halo stars that have [O/H] ≤ -2.0, and

calculated the deviations about this line for both stars and DLAs. A Kolmogorov–Smirnov (KS) test between the calculated deviations reveals a 75 per cent chance that both VMP stars and DLAs are drawn from the same population, which is inconclusive given the present statistics. For this test we have used the C/O values in halo stars that were derived assuming efficient hydrogen collisions (with a scaling factor $S_{\rm H} = 1$; see footnote 9). If instead we adopt the stellar values derived for inefficient collisions ($S_{\rm H} = 0$), we find a 90 per cent chance that both samples are drawn from the same population. Such good agreement between halo stars and DLAs does not support the recent claim by Tsujimoto & Bekki (2011), who suggest that the IMF of the stars that enriched metal-poor DLAs is different from the IMF of the stars that enriched Galactic halo stars with their metals. The good general agreement we find between stars and DLAs – both exhibiting an elevated C/O ratio at the lowest metallicities probed – points to a universal origin for their C/O 'excess' in this regime.

6.2 The O/Fe debate in the metal-poor regime

We now turn to the relative abundances of oxygen and iron at low metallicity. Whilst we cannot do justice to the extensive literature on this topic, we outline below the basic facts that are relevant to our discussion, and direct the interested reader to the comprehensive review by McWilliam (1997).

The largest oxygen yield comes from the most massive stars that explode as SNe II. The production of iron, on the other hand, is largely from SNe Ia which typically explode $\sim$1 Gyr later (see e.g. Greggio 2010).[10] Therefore, at early times (when the metallicity is low), one expects O to be enhanced relative to Fe. At later times, when the delayed contribution of Fe from SNe Ia kicks in, there is a break in the O/Fe trend which is then expected to decrease. Thus, the relative abundance of O and Fe allows us to measure the relative contribution of SNe Ia and SNe II (see e.g. the qualitative discussion by Wheeler, Sneden & Truran 1989).

In the Milky Way, the break in [O/Fe] occurs roughly at [Fe/H] $\simeq -1.0$. Whilst there is sound agreement regarding the nature of the trend in [O/Fe] when [Fe/H] $\gtrsim -1.0$, the behaviour of [O/Fe] when [Fe/H] $\lesssim -1.0$ is less certain. This disagreement stems from the uncertainty of the oxygen abundances measured in metal-poor stars: there are four different indicators of the oxygen abundance, and to some extent they all disagree with one another in the metal-poor regime (García Pérez et al. 2006).

Perhaps the most reliable [O/H] indicator at low metallicity is the forbidden [O I] λ6300 line which, despite being subject to 3D corrections of ~ -0.2 dex when [Fe/H] ~ -2.0 (Nissen et al. 2002; Collet, Asplund & Trampedach 2007), is known to form in LTE (Asplund 2005). Unfortunately, this line becomes very weak when [Fe/H] < -2.0 and its detection requires data of high S/N. After accounting for 3D corrections to the O abundance, most authors conclude that the O/Fe ratio is approximately constant at [O/Fe] $\simeq +0.4$ for [Fe/H] $\lesssim -1$ (Nissen et al. 2002; Cayrel et al. 2004; García Pérez et al. 2006), with perhaps a slight increase towards the lowest metallicities.

The most commonly used diagnostic for measuring [O/H] in stars is the O I triplet near 777 nm ($\lambda = 7771.9$, 7774.2, 7775.4 Å), despite the fact that it suffers from large non-LTE corrections (Fabbian et al. 2009b). However, contrary to the nearly constant value of [O/Fe] below [Fe/H] $\lesssim -1$ deduced from the [O I] λ6300 line, an LTE analysis of the O I triplet leads to a quasi-linear increase in [O/Fe] with decreasing metallicity (see e.g. Fulbright & Johnson 2003). This discrepancy is often blamed on the uncertain (negative) non-LTE corrections to the O I triplet. In order to make headway with the [O/Fe] conflict, Fabbian et al. (2009b) performed a detailed non-LTE analysis of the O I triplet, and found corrections amounting to $\gtrsim$0.5 dex when [Fe/H] $= -3.0$, increasing rapidly at lower metallicities (see also Fabbian et al. 2009a). After accounting for such corrections, Fabbian et al. (2009b) concluded that almost all diagnostics are now conceivably consistent, and that [O/Fe] exhibits a roughly flat plateau with values between +0.4 and +0.6 when [Fe/H] $\lesssim -1$.

In contrast to the profusion of stellar studies of [O/Fe] in the VMP regime, this ratio has received relatively little attention in DLAs so far. The reason is that the most readily available O I absorption lines are almost always saturated, and the weakest lines are often blended with unrelated absorption in the Lyα forest (Prochaska & Wolfe 2002). For these reasons, several authors have investigated the [O/Fe] trend in sub-DLAs, where the O I absorption lines are weaker (Péroux et al. 2003b; O'Meara et al. 2005). However, uncertain negative ionization corrections to the Fe II lines might become important for such systems, complicating the interpretation. Other authors have instead used [S/Zn] as a proxy for [O/Fe] (Nissen et al. 2007), but these lines become too weak in the VMP regime.

In fact, there have only been two studies in the literature that consider [O/Fe] in DLAs. The first was conducted by Petitjean et al. (2008), who reported an [O/Fe] plateau of $+0.32 \pm 0.10$ from their sample of 13 DLAs with [Fe/H] < -1.0 (three of which have [Fe/H] < -2.0). The second, more recent, study was conducted by Penprase et al. (2010) whose sample includes five DLAs with [Fe/H] < -2.0. Their measurements, however, have large uncertainty ($\sim \pm 0.4$ dex), so it is difficult to discern the underlying trend.

Our survey constitutes the largest sample of high-resolution measures of O I and Fe II absorption in DLAs. The [O/Fe] values are plotted in Fig. 11 where, for comparison, we also show a selection of [O/Fe] measurements in Galactic stars based on the forbidden [O I] λ6300 line (Nissen et al. 2002; Cayrel et al. 2004; García Pérez et al. 2006) with 3D corrections applied as we now describe.

The [O I] λ6300 line corresponds to a forbidden transition between two levels of the ground configuration of the O I atom, which are closely coupled via collisions. Because nearly all oxygen atoms are in the ground state in the atmospheres of late-type stars, one expects LTE to prevail; this is confirmed by detailed statistical equilibrium calculations (Kiselman 1993). Non-LTE effects on the derived iron abundances are also negligible, when lines from the dominating ionization stage (Fe II) are considered (Mashonkina et al. 2011). The 3D–1D corrections are, however, significant for metal-poor stars; [O/H] derived from the [O I] λ6300 line decreases and [Fe/H] from Fe II lines increases slightly. As calculated by Nissen et al. (2002), the net effect on [O/Fe] for metal-poor main-sequence stars can be approximated by the expression $[{\rm O/Fe}]_{\rm 3D} - [{\rm O/Fe}]_{\rm 1D} = 0.11\,[{\rm Fe/H}]$, whereas $[{\rm Fe/H}]_{\rm 3D} - [{\rm Fe/H}]_{\rm 1D} = -0.04\,[{\rm Fe/H}]$. Cayrel et al. (2004) assumed that the same corrections are also valid for metal-poor red giants. We have verified that this is approximately correct by applying 3D corrections for giant stars as calculated by Collet et al. (2007) for the [O I] λ6300 line and the Fe lines used by Cayrel et al. (2004). The same 3D corrections are then also expected for the cool sub-giants studied by García Pérez et al. (2006), because they have atmospheric parameters intermediate between

[10] Iron may also be contributed by SNe Ia that 'promptly' explode at early times ($\sim$0.1 Gyr). For the relevant details, we direct the interested reader to the discussion by Mannucci, Della Valle & Panagia (2006).

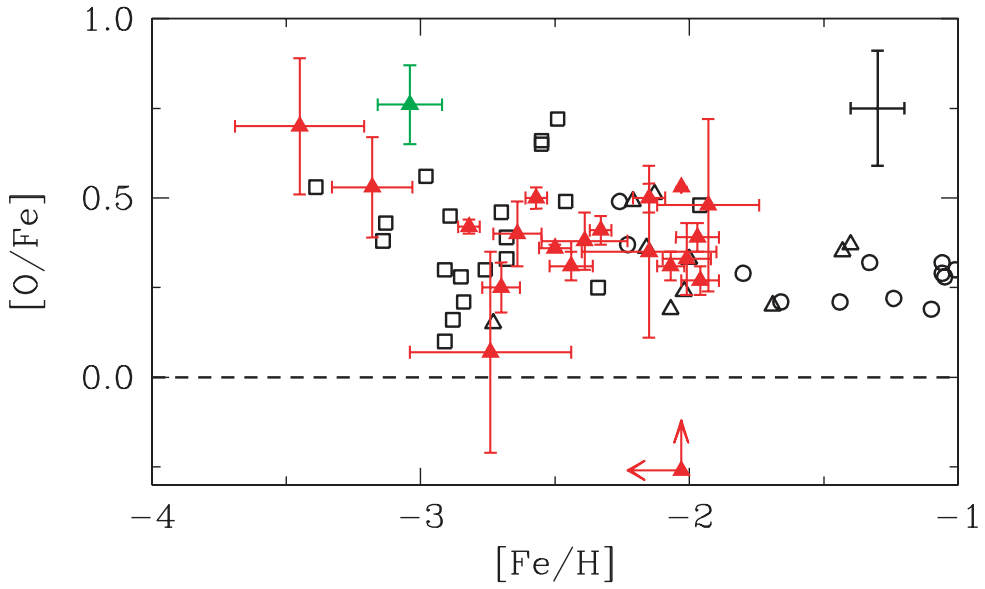

Figure 11. The [O/Fe] ratio in VMP DLAs (filled red triangles) where [O/H] has been measured from high-resolution spectra. The green triangle refers to the carbon-enhanced DLA reported by Cooke et al. (2011); the upper limit on [Fe/H] and corresponding lower limit on [O/Fe] (red triangle with arrows) are for the DLA towards J0311−1722 where Fe II absorption is not detected. The VMP DLA sample is compared with the stellar abundance measurements by Nissen et al. (2002) (circles), Cayrel et al. (2004) (squares) and García Pérez et al. (2006) (triangles), all based on the [O I] λ6300 line and corrected for 3D effects (see text for further details). The error bars at the top-right corner of the plot indicate the typical errors in the stellar abundance measurements. All the measurements in this plot are tabulated, together with their individual errors, in Appendix B.

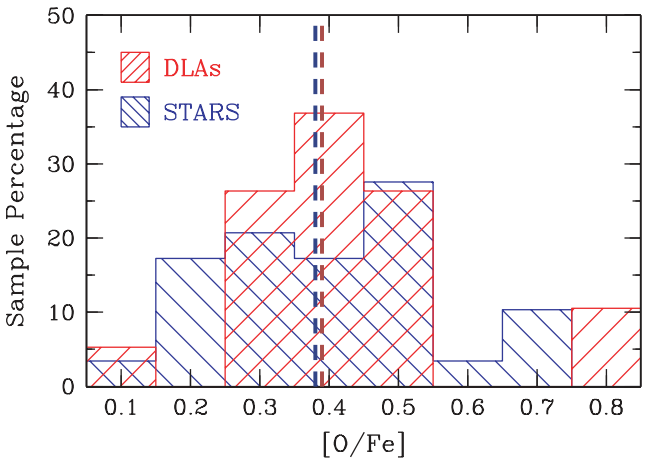

Figure 12. The distribution of [O/Fe] values (where [Fe/H] ≤ −2.0) in DLAs for our sample (red histogram) as compared to the compilation of [O/Fe] in stars measured from the [O I] λ6300 line (blue histogram). The dashed vertical red and blue lines indicate the median values for DLAs and stars respectively, corresponding to a difference of only ∼0.01 dex.

those of the main-sequence and red giant stars. For reference, we list in Appendix B values of [O/Fe] and [Fe/H] corrected for 3D effects, as well as the [O/Fe] and [Fe/H] values measured in our sample of VMP DLAs.

Once the above-mentioned 3D corrections are applied, it can be seen that stars and DLAs share a similar trend of [O/Fe] with decreasing metallicity. To illustrate this point, we show the two samples (where [Fe/H] ≤ −2.0) as histograms in Fig. 12. A KS test[11] reveals that the probability the two data sets are drawn from the same parent population is 71 per cent.

[11] We have not included the star CS 22949−037 in this test (from Cayrel et al. 2004), since it exhibits a peculiar abundance pattern, with [O/Fe] = +1.54.

The DLA values of [O/Fe] exhibit relatively little scatter given the errors. In the range −3 ≤ [Fe/H] ≤ −2, [O/Fe] is consistent with a constant value: $[\langle O/Fe\rangle] = +0.35 \pm 0.09$. This is in good agreement with the mean value reported by Petitjean et al. (2008), $[\langle O/Fe\rangle] = +0.32 \pm 0.10$, for $-2.0 \lesssim$ [Fe/H] $\lesssim -1.0$. Interestingly, there may be a hint in our data that [O/Fe] increases further when [Fe/H] $\lesssim -3$ (see Fig. 11), which would presumably be indicative of a contribution from more massive stars. However, more data are required to confirm this 'trend' which at present is suggested by the two most metal-poor DLAs in our sample. For the moment, we simply conclude that the 'cosmic' trend of [O/Fe] in the VMP regime (−3 ≤ [Fe/H] ≤ −2) reaches a plateau of ∼+0.35, and is remarkably tight, especially given the observational errors.

In closing, the DLA measurements of [O/Fe] help resolve the controversy regarding the relative abundances of O and Fe in metal-poor Galactic stars. It is plausible that VMP DLAs harbour the reservoir of neutral gas that will later condense to form a population of VMP stars. It is thus expected that towards the lowest metallicities both stars and DLAs should exhibit a similar trend. We conclude that, unless there are marked differences between the chemical evolution histories of DLAs and the early Galaxy, our results and those of Petitjean et al. (2008) favour an approximately constant plateau of stellar [O/Fe] values when [Fe/H] $\lesssim -1$, with perhaps a mild increase with decreasing [Fe/H]. In any case, given the on-going improvement in the accuracy of the stellar models and the increasing samples of VMP DLAs, we anticipate that this issue may well be settled in the near future.

7 DISCUSSION

7.1 The typical VMP DLA

With the large sample of measurements we have assembled, we can now attempt to reconstruct the abundance pattern of a 'typical' VMP DLA, and to consider the clues it may provide on the

Table 13. The mean value and dispersion in X/O for each element of the VMP DLAs in our sample.

X	$[\langle X/O\rangle]$	$\sigma_{[\langle X/O\rangle]}$	$n_{[\langle X/O\rangle]}$
C	−0.28	0.12	9
N	−1.05	0.19	13
Al	−0.44	0.13	11
Si	−0.08	0.10	21
Fe	−0.39	0.12	20

nucleosynthesis by the earliest generation of stars. To achieve this goal, we are obviously required to select a reference element other that H, as we have no means to determine how much H was mixed with the nucleosynthetic products from the earliest generations of stars. Rather, the ratio of two *metals* provides the best handle for determining the properties of the generation of stars from which they were synthesized.

With our goal to probe early nucleosynthesis borne in mind, the most appropriate reference element is O, for the following reasons: (1) the dominant O yield comes from a single source – massive stars. Thus, the origin of O is well-understood; (2) O is the most abundant metal in the Universe; and (3) at the lowest metallicities, where we expect to uncover the signature from early nucleosynthesis, several O lines become unsaturated in DLAs. Thus, it is relatively straightforward to measure [O/H]. Taking oxygen then as the reference element, we have constructed the typical abundance pattern for a VMP DLA by determining the mean $\langle X/O\rangle$ ratio for each available element, X, and then referring this mean value to the adopted solar scale (i.e. we take the log of the mean, $[\langle X/O\rangle]$). These mean values are listed in Table 13 along with the dispersion in the available measurements ($\sigma_{[\langle X/O\rangle]}$). In the last column of Table 13, we indicate the total number of DLAs that were used in determining the mean X/O.

The corresponding abundance pattern is illustrated in Fig. 13. In the following subsection, we investigate the most likely origin of the metals in VMP DLAs by directly comparing this typical abundance pattern to model yield calculations of both Population II and Population III stars. Before continuing, however, it is important to keep in mind that the 'typical' $[\langle N/O\rangle]$ in Table 13 may be biased high, because it does not include a number of upper limits, where the N I lines are too weak to be measured. As discussed above (Section 6.1), it is also possible that $[\langle C/O\rangle]$ may be biased towards lower values than the true mean.

According to our sample definition (see Section 4.8), this 'typical' abundance pattern is based on DLAs where [Fe/H] ≤ -2.0. By restricting this sample to only contain DLAs with [Fe/H] ≤ -2.5, we found that the typical abundance for all elements considered here changes by no more than 0.02 dex, except in the case of $[\langle N/O\rangle]$, which is lower by 0.14 dex. Thus, our choice of metallicity cut does not introduce a significant bias into the typical VMP DLA abundance pattern.

7.2 Clues to early episodes of nucleosynthesis

There is increasing evidence to suggest that the most metal-poor DLAs may retain the signature from the earliest episodes of star formation (Erni et al. 2006; Pettini et al. 2008; Cooke et al. 2011). In this picture, the most metal-poor DLAs condensed directly out of material that was enriched by either: (1) an external halo that distributed its products over large cosmological volumes via multi-

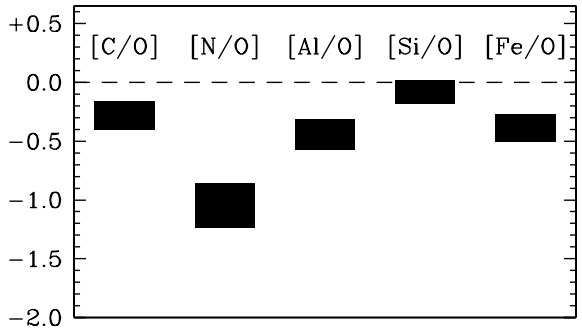

Figure 13. The abundance pattern of a typical VMP DLA is illustrated by the black boxes, where the height in each box represents the dispersion in the population. The dashed line corresponds to the solar abundance ratios.

SN events (Madau, Ferrara & Rees 2001); or perhaps (2) just a few SNe from the halo in which the DLA now resides (Bland-Hawthorn et al. 2011).

Cosmological simulations of galaxy formation support the possibility that such DLAs still retain the chemical signature of early enrichment (Pontzen et al. 2008; Tescari et al. 2009); the most metal-poor DLAs arise in low-mass haloes that have undergone little to no *in situ* star formation. It is possible, however, that VMP DLAs acquired some of their metals at later times from nearby sources that delivered metals into the IGM via galactic superwinds (see e.g. Oppenheimer & Davé 2008), which may complicate the interpretation. Perhaps the most straightforward way to discriminate between these enrichment scenarios is to compare the model yields of both Population III and Population II stars with that of the typical VMP DLA described in Section 7.1.

We consider three sources that could be responsible for the metals in VMP DLAs: (1) massive metal-free stars, with main-sequence masses in the range 140–260 $M_\odot$ that explode as pair-instability supernovae (PISNe; Heger & Woosley 2002); (2) massive metal-free stars, with progenitor masses in the range 10–100 $M_\odot$ that explode as core-collapse supernovae (CCSNe; Heger & Woosley 2010); and (3) massive Population II (and I) stars, with progenitor masses in the range 13–35 $M_\odot$, covering a range in metallicity (Chieffi & Limongi 2004), also ending their lives as CCSNe. To determine the dominant source of the metals in VMP DLAs, we integrate these model yields over a Salpeter-like power-law IMF, $dN/dM \propto M^{-(1+\gamma)}$ (where $\gamma = 1.35$ for a Salpeter IMF), and consider three values for the power-law index in the case of zero metallicity ($\gamma = 1.35, 2.35, 3.35$). For massive Population II stars, we consider only a Salpeter IMF, with $\gamma = 1.35$. The results of these calculations are shown in Fig. 14.

Let us first consider the yields from metal-free stars with masses in the range 140–260 $M_\odot$. These stars explode as PISNe, the physics of which is well-understood (Heger & Woosley 2002; Umeda & Nomoto 2002). The calculated yields from PISNe are thus the least model dependent of the three cases considered here. Qualitatively, these models could have been ruled out on the basis of the near-solar [Si/O] that is typical of the VMP DLA population; PISNe are expected to yield supersolar [Si, S, Ar, Ca/O]. Indeed, for the range of γ considered here, such SNe provide a poor fit to the typical VMP DLA population (top panel of Fig. 14).

We now turn to models of massive stars (10–100 $M_\odot$) that end their lives as CCSNe. Unfortunately, the explosion mechanism of CCSNe is poorly understood, and several unknown physical effects need to be parametrized and suitably adjusted to find the best solution for a given set of data. In particular, one usually parametrizes

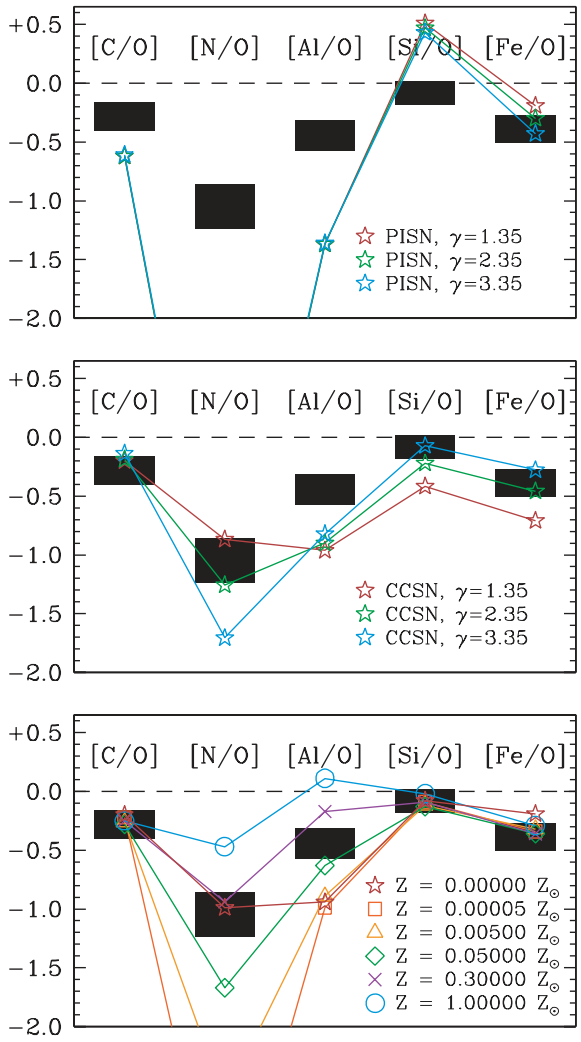

Figure 14. The abundance pattern of the 'typical' VMP DLA (black boxes; cf. Fig. 13) is compared to nucleosynthesis models of massive stars (symbols connected by lines). Top panel: the symbols represent the yields from PISNe of zero-metallicity stars (Heger & Woosley 2002) for three indices of a power-law IMF (red, green, blue correspond to $\gamma = 1.35, 2.35, 3.35$, respectively). Middle panel: same as above, except for CCSNe models of zero-metallicity stars (Heger & Woosley 2010). Bottom panel: comparing the typical DLA abundance pattern with the model explosive yields of massive Population II stars (Chieffi & Limongi 2004). A range of metallicities are considered, as indicated by the accompanying legend. In all cases for this bottom panel, we plot the integrated yields from the Salpeter IMF with a power-law index of $\gamma = 1.35$.

the explosion energy, the degree of mixing between the stellar layers during the explosion and the amount of material that falls back on to the central remnant.

The most recent suite of published CCSNe yields for metal-free stars are those by Heger & Woosley (2010). These computations provide a detailed account of the nucleosynthetic products over a large range of progenitor masses (10–100 $M_\odot$) with a typical mass resolution of 0.1 $M_\odot$. As part of their study, Heger & Woosley (2010) compiled a data base of these model yields that are imported into their STARFIT[12] software. This software is designed to objectively sieve through the vast parameter space and select the explosion parameters that best fit the data.

To maintain consistency with the other yield models that are considered here, we compare the abundance pattern of the typical VMP DLA to the expected yields for the three power-law indices of a Salpeter-like IMF ($\gamma = 1.35, 2.35, 3.35$). We therefore froze the remaining parameters to the 'standard' case, which corresponds to a constant explosion energy (1.2×10^{51} erg) for all masses in the range 10–100 $M_\odot$ (see Heger & Woosley 2010 for further details). This standard case sets the piston location of the explosion to be at the base of the oxygen burning shell (where the entropy per baryon $\simeq$4), and applies a mixing boxcar filter with a width which is 10 per cent the He core size. The material that falls back on to the central remnant is not parametrized in this code, but is instead calculated by switching the piston off 100 s after the explosion and defining an inner boundary condition where material is accreted.

All three fits are reproduced in the middle panel of Fig. 14. The 'standard' case with the yields from metal-free stars seems to produce a reasonable agreement with the observed metal ratios in the 'typical' VMP DLA, although Al is discrepant by $\sim$0.5 dex and, interestingly, IMF slopes steeper than Salpeter seem to fit the data best. Of course, by relaxing some of the default constraints it may be possible to improve the fit further, but we have refrained from doing so, given that there are still many uncertainties in accurately modelling the physics behind the explosion. Some of these uncertainties are only now beginning to be addressed in some detail (see Joggerst, Almgren & Woosley 2010b, and references therein).

Finally, we consider the set of model CCSNe yields published by Chieffi & Limongi (2004), which allow us to test whether or not Population II stars can also account for the origin of the metals in VMP DLAs. Before comparing the models by Chieffi & Limongi to the typical VMP DLA, it is worth noting the important differences between this code and the one described above by Heger & Woosley (2010). Aside from the obvious difference in metallicity, the models by Chieffi & Limongi (2004) target the mass range 13–35 $M_\odot$ with a relatively coarser mass resolution of 5 $M_\odot$. In addition, this code parametrizes the amount of material that falls back on to the central remnant. In their standard case, this prescription requires 0.1 $M_\odot$ of ^{56}Ni to be ejected from the star, and thus all material interior to this mass coordinate is 'accreted' by the remnant. Finally, this code is yet to implement a 'mixing parameter' to model the mixing that takes place between the stellar layers during the SN explosion. Adopting their standard case, which has an explosion energy of 1.2×10^{51} erg, we integrate the model yields over a Salpeter-like IMF with $\gamma = 1.35$. The results are shown in the bottom panel of Fig. 14.

These calculations adopt an initial chemical composition that is simply scaled from the solar abundance pattern. According to Chieffi & Limongi (2004), the model yields for stars with an initial metallicity of $Z \leq 0.005$ $Z_\odot$ are not strongly dependent on the initial composition of the star. It is important to note, however, that by introducing an α-enhancement to the initial metallicity (which is perhaps more realistic than simply scaling the solar abundance pattern), the yields for the odd atomic number elements are increased (see their fig. 1). Thus, our calculations may underestimate the N/O and Al/O ratios. Furthermore, at higher metallicities ($Z > 0.005$ $Z_\odot$), the yields *do* depend on the initial composition of the stars.

Inspecting the bottom panel of Fig. 14, it can been seen that, at face value, the $Z/Z_\odot = 0.0, 0.05$ and 0.3 models provide reasonable fits to the abundance pattern of a typical VMP DLA. We also note the broad agreement between the metal-free models by Heger & Woosley (2010) and Chieffi & Limongi (2004). On the other hand,

[12] STARFIT is written with the INTERACTIVE DATA LANGUAGE software and is available from: http://homepages.spa.umn.edu/~alex/znuc/

the $Z/Z_{\odot} = 0.05$ and 0.3 models also seem to provide reasonable fits to the abundance pattern. However, once the stars have reached metallicities greater than 1/20 of solar, the metal ratios in the gas should be compared with the predictions of full chemical evolution models which are beyond the scope of this paper.

Given the current (largely) model-dependent nature of these calculations, we are unable to draw firm conclusions at this stage. Whilst the above models suggest that metal-free stars could have synthesized the metals that now reside in VMP DLAs, we cannot rule out the possibility that Population II stars are also responsible. We suspect that it will be necessary to measure the abundances of additional metals in order to better distinguish between Population II and Population III models, since the ratios of the most abundant elements ([C/O], [Si/O] and [Fe/O]) provide the weakest constraints on the nature of the objects that synthesized them. Some of the largest differences between these models are exhibited by the iron-peak elements, and in particular, Ti, Ni and Zn. The detection of these rarer elements in the most metal-poor DLAs will have to wait for the advent of the next generation of extremely large optical telescopes.

Finally, we note that the models used here to compare with a typical VMP DLA are still quite dependent on unknown physics; the single largest uncertainty in these models is the explosion mechanism. Additional physics also needs to be included, such as the mixing induced by stellar rotation (Meynet, Ekström & Maeder 2006; Hirschi 2007; Meynet et al. 2010; Joggerst et al. 2010a) and the Rayleigh–Taylor instability (Joggerst, Woosley & Heger 2009). These effects will presumably be considered in the next generation of fine-grid nucleosynthesis models, when the limitations of computing power will hopefully be less of a concern.

7.3 Comparison with data of medium spectral resolution

Finally, we compare DLA abundance determinations obtained from high ($R \sim 40\,000$) and medium ($R \sim 5000$) spectral resolution data. Such a comparison is motivated by the realization that, even with efficient echelle spectrographs on 8–10 m telescopes, it is typically necessary to integrate on a single QSO for the equivalent of one night in order to obtain the S/N required to measure elemental abundances from high-resolution spectra. By settling for lower resolutions, the exposure times are greatly reduced; for example, most of the QSOs in the survey by Penprase et al. (2010) were observed for about one hour with the Echelle Spectrograph and Imager (ESI). Clearly, it is of interest to test how similar the abundance measurements are for the most metal-poor DLAs, if we were to forgo the accuracy of high spectral resolution in order to secure a larger sample.

In this context, there are two main concerns that potentially limit the accuracy of abundance measurements from medium (as opposed to high) spectral resolution data. First, VMP DLAs typically have linewidths $\lesssim 10\,\mathrm{km\,s^{-1}}$ (Ledoux et al. 2006; Murphy et al. 2007; Prochaska et al. 2008), which are unresolved at $R = 5000$. One must therefore appeal to a curve-of-growth analysis appropriate to a single absorbing cloud, which is often an oversimplification (see our Table 2, and also Prochaska 2006). Secondly, the relevant absorption lines may be saturated, and the degree of saturation may be difficult to estimate correctly, even with a well-defined curve-of-growth.

As it happens, three VMP DLAs from the present work are in common with the lower resolution survey of Penprase et al. (2010), providing us with the means to compare column densities from the two sets of spectra, as in Table 14. For two of the DLAs, J0831+3358 and J1037+0139, Penprase et al. (2010) reported lower limits on the column densities of the available metal ions. As can be seen from Table 14, while these lower limits are always consistent with the values measured from our echelle spectra, they fall short of the true column density by widely differing amounts, from as little as -0.13 dex to as much as -0.72 dex. This wide range significantly reduces the usefulness of the lower limits.

Table 14. Column densities estimated from high and medium resolution spectra.

Ion	$\log N^{a}_{\rm coo}$	$\log N^{b}_{\rm pen,m}$	$\log N^{c}_{\rm pen,c}$
	J0831+3358		
Al II	12.19 ± 0.06	...	>11.56
Si II	13.75 ± 0.04	...	>13.03
Fe II	13.33 ± 0.06	...	>13.13
	J1001+0343		
C II	13.58 ± 0.02	13.63 ± 0.06	13.76 ± 0.13
O I	14.25 ± 0.02	13.90 ± 0.07	13.98 ± 0.08
Si II	12.86 ± 0.01	12.70 ± 0.05	12.82 ± 0.12
	J1037+0139		
O I	15.06 ± 0.04	...	>14.48
Al II	12.32 ± 0.03	...	>12.09
Si II	13.97 ± 0.03	...	>13.69
Fe II	13.53 ± 0.02	...	>13.33

[a]Our results.
[b]Column densities measured by Penprase et al. (2010).
[c]Column density estimates by Penprase et al. (2010) after applying a saturation correction.

Turning now to the DLA at $z_{\rm abs} = 3.07841$ towards J1001+0343, we recall that our UVES spectra show that the absorption arises in a single component with Doppler parameter $b = 7.0 \pm 0.1\,\mathrm{km\,s^{-1}}$ (see Fig. 3). This value is not too dissimilar from $b = 7.5\,\mathrm{km\,s^{-1}}$ estimated by Penprase et al. (2010) from a curve-of-growth analysis. Indeed, the two analyses give consistent estimates of the Si II column density [after Penprase et al. (2010) apply a saturation correction]. The C II and O I lines, however, tell a different story. For this DLA, Penprase et al. (2010) need not have applied a saturation correction to the C II λ1334 line, since it is not strongly saturated (see Fig. 3). Indeed, prior to applying such a correction, their column density estimate was in broad agreement with that derived here. Conversely, O I λ1302 is closer to saturation and, even with the correction applied by Penprase et al. (2010), these authors' estimate falls short of the value deduced here by nearly a factor of 2. The combined effect is an overestimate of [C/O] by 0.45 dex.

Based on this example, there appear to be non-negligible uncertainties in the derivation of element ratios from spectra at $R \sim 5000$. While these uncertainties did not affect the principle goal of the study by Penprase et al. (2010) – to uncover the most metal-poor DLAs – it would appear that high-resolution observations are indeed necessary to measure element abundances in VMP DLAs with an accuracy better than a factor of $\sim$2.

8 SUMMARY AND CONCLUSIONS

We have conducted a survey for VMP DLAs to shed light on the earliest episodes of nucleosynthesis in our Universe. Our sample includes seven new DLAs observed with high-resolution spectrographs ($R \gtrsim 30\,000$); when combined with the five metal-poor DLAs previously reported from this programme (Pettini et al. 2008; Cooke et al. 2011) and an additional 10 DLAs from the

literature, it constitutes the largest survey to date for DLAs with a metallicity [Fe/H] < -2.0. From the analysis of these data, we draw the following conclusions.

(i) Having now doubled the sample of DLAs where the C/O ratio is measured from unsaturated absorption lines, we confirm that DLAs exhibit near-solar values of C/O at the lowest metallicities probed. Furthermore, we find good agreement in the C/O ratio observed in our sample of DLAs and in recent compilations of the most metal-poor Galactic halo stars. We argue that such good agreement points to a universal origin for the C/O 'excess' in this regime.

(ii) For the first time, we investigate the [O/Fe] ratio in VMP DLAs. For 20 DLAs with [Fe/H] < -2.0, we find a small dispersion around a mean value $[\langle \mathrm{O/Fe} \rangle] = +0.39 \pm 0.12$. We have also presented tentative evidence for a rise in the [O/Fe] ratio when [Fe/H] $\lesssim -3.0$.

(iii) In view of the long-standing debate as to the behaviour of the [O/Fe] ratio in metal-poor Galactic halo stars, we have compared the stellar trend to that observed in our sample of DLAs. We find good agreement between stars and DLAs when the stellar oxygen abundance is measured from the [O I] λ6300 line (after correcting for 3D effects). Based on the available DLA samples, we conclude that [O/Fe] is essentially flat in the metallicity interval $-3.0 \lesssim$ [Fe/H] $\lesssim -1.0$, with the possibility of an increase at yet lower metallicities.

(iv) We have constructed the abundance pattern of a typical VMP DLA for the five most commonly observed metals, using O as a reference. We find that Si/O is just below solar ($[\langle \mathrm{Si/O} \rangle] = -0.08$), whilst $[\langle \mathrm{C/O} \rangle] = -0.28$ and $[\langle \mathrm{Fe/O} \rangle] = -0.39$. The largest deviations from a solar scaled abundance pattern are exhibited by N and Al, with $[\langle \mathrm{N, Al/O} \rangle] = -1.05, -0.44$.

(v) One of the main aims of this work was to investigate the origin of the metals in the most metal-poor DLAs. To achieve this goal, we compared the abundance pattern of a 'typical' VMP DLA with those expected from model calculations using the yields of Population II and Population III stars. For the few elements considered here, we find a reasonable agreement between the abundance pattern of the typical VMP DLA and the 'standard model' of a population of metal-free stars (i.e. a top-heavy IMF where all stars explode as CCSNe with an energy of 1.2×10^{51} erg). However, given that we only have access to a handful of metals, we cannot unambiguously rule out (an additional contribution from) more metal-rich Population II stars. On the other hand, we are able to firmly conclude that the typical VMP DLA was not solely enriched by PISNe from very massive metal-free stars.

Our ongoing programme to measure the abundances in the most metal-poor DLAs complements local studies of Galactic metal-poor halo stars. The good agreement we have found between these two populations suggests a universal origin for their metals. The results presented here emphasize the importance of measuring elemental abundances in the most metal-poor DLAs; these systems present us with a unique window of opportunity to probe the nucleosynthesis by some of the earliest structures in the Universe.

ACKNOWLEDGMENTS

We are grateful to the relevant time assignment committees for their continuing support of this demanding observational programme, and to the staff astronomers at the VLT and Keck Observatories for their competent assistance with the observations. We also thank an anonymous referee who provided valuable comments that improved the presentation of this work. Tom Barlow and Michael Murphy generously shared their echelle data reduction software. Valuable advice and help with various aspects of the work described in this paper was provided by Bob Carswell, Paul Hewett and Regina Jorgenson. We thank the Hawaiian people for the opportunity to observe from Mauna Kea; without their hospitality, this work would not have been possible. RC is jointly funded by the Cambridge Overseas Trust and the Cambridge Commonwealth/Australia Trust with an Allen Cambridge Australia Trust Scholarship. CCS's research is partly supported by grants AST-0606912 and AST-0908805 from the US National Science Foundation.

REFERENCES

Akerman C. J., Carigi L., Nissen P. E., Pettini M., Asplund M., 2004, A&A, 414, 931
Akerman C. J., Ellison S. L., Pettini M., Steidel C. C., 2005, A&A, 440, 499
Aoki W., Beers T. C., Christlieb N., Norris J. E., Ryan S. G., Tsangarides S., 2007, ApJ, 655, 492
Asplund M., 2005, ARA&A, 43, 481
Asplund M., Grevesse N., Sauval A. J., Scott P., 2009, ARA&A, 47, 481
Becker G. D., Sargent W. L. W., Rauch M., Simcoe R. A., 2006, ApJ, 640, 69
Becker G. D., Sargent W. L. W., Rauch M., Calverley A. P., 2011, ApJ, 735, 93
Beers T. C., Christlieb N., 2005, ARA&A, 43, 531
Bensby T., Feltzing S., 2006, MNRAS, 367, 1181
Bland-Hawthorn J., Sutherland R., Karlsson T., 2011, EAS Publ. Ser., 48, 397
Bromm V., Larson R. B., 2004, ARA&A, 42, 79
Bromm V., Loeb A., 2003, Nat, 425, 812
Carollo D., Beers T. C., Bovy J., Sivarani T., Norris J. E., Freeman K. C., Aoki W., Lee Y. S., 2011, preprint (arXiv:1103.3067)
Cayrel R. et al., 2004, A&A, 416, 1117
Chiappini C., Hirschi R., Meynet G., Ekström S., Maeder A., Matteucci F., 2006, A&A, 449, L27
Chieffi A., Limongi M., 2002, ApJ, 577, 281
Chieffi A., Limongi M., 2004, ApJ, 608, 405
Christlieb N. et al., 2002, Nat, 419, 904
Collet R., Asplund M., Trampedach R., 2007, A&A, 469, 687
Cooke R., Pettini M., Steidel C. C., Rudie G. C., Jorgenson R. A., 2011, MNRAS, 412, 1047
Dekker H., D'Odorico S., Kaufer A., Delabre B., Kotzlowski H., 2000, Proc. SPIE, 4008, 534
Dessauges-Zavadsky M., D'Odorico S., McMahon R. G., Molaro P., Ledoux C., Péroux C., Storrie-Lombardi L. J., 2001, A&A, 370, 426
Dessauges-Zavadsky M., Péroux C., Kim T.-S., D'Odorico S., McMahon R. G., 2003, MNRAS, 345, 447
Drawin H. W., 1969, Z. Phys., 225, 483
Ellison S. L., Prochaska J. X., Hennawi J., Lopez S., Usher C., Wolfe A. M., Russell D. M., Benn C. R., 2010, MNRAS, 406, 1435
Erni P., Richter P., Ledoux C., Petitjean P., 2006, A&A, 451, 19
Fabbian D., Nissen P. E., Asplund M., Pettini M., Akerman C., 2009a, A&A, 500, 1143
Fabbian D., Asplund M., Barklem P. S., Carlsson M., Kiselman D., 2009b, A&A, 500, 1221
Ferland G. J., Korista K. T., Verner D. A., Ferguson J. W., Kingdon J. B., Verner E. M., 1998, PASP, 110, 761
Field G. B., Steigman G., 1971, ApJ, 166, 59
Frebel A., 2010, Astron. Nachr., 331, 474
Frebel A. et al., 2005, Nat, 434, 871
Frebel A., Johnson J. L., Bromm V., 2007, MNRAS, 380, L40
Fulbright J. P., Johnson J. A., 2003, ApJ, 595, 1154

García Pérez A. E., Asplund M., Primas F., Nissen P. E., Gustafsson B., 2006, A&A, 451, 621
Greggio L., 2010, MNRAS, 406, 22
Haardt F., Madau P., 2001, in Neumann D. M., Tran J. T. V., eds, XXIst Moriond Astrophys. Meeting, Clusters of Galaxies and the High Redshift Universe Observed in X-ray Frontières, Paris, p. 64
Heger A., Woosley S. E., 2002, ApJ, 567, 532
Heger A., Woosley S. E., 2010, ApJ, 724, 341
Hirschi R., 2007, A&A, 461, 571
Jenkins E. B., Tripp T. M., 2006, ApJ, 637, 548
Joggerst C. C., Woosley S. E., Heger A., 2009, ApJ, 693, 1780
Joggerst C. C., Almgren A., Bell J., Heger A., Whalen D., Woosley S. E., 2010a, ApJ, 709, 11
Joggerst C. C., Almgren A., Woosley S. E., 2010b, ApJ, 723, 353
Jorgenson R. A., Wolfe A. M., Prochaska J. X., Carswell R. F., 2009, ApJ, 704, 247
Karlsson T., Bromm V., Bland-Hawthorn J., 2011, preprint (arXiv:1101.4024)
Kiselman D., 1993, A&A, 275, 269
Ledoux C., Petitjean P., Srianand R., 2003, MNRAS, 346, 209
Ledoux C., Petitjean P., Fynbo J. P. U., Møller P., Srianand R., 2006, A&A, 457, 71
Lodders K., Plame H., Gail H.-P., 2009, in Trümper J. E., ed., Landolt-Börnstein, New Series, Abundances of the Elements in the Solar System. Springer-Verlag, Berlin, p. 44
Madau P., Ferrara A., Rees M. J., 2001, ApJ, 555, 92
Mannucci F., Della Valle M., Panagia N., 2006, MNRAS, 370, 773
Mashonkina L., Gehren T., Shi J.-R., Korn A. J., Grupp F., 2011, A&A, 528, A87
McWilliam A., 1997, ARA&A, 35, 503
Meynet G., Ekström S., Maeder A., 2006, A&A, 447, 623
Meynet G., Hirschi R., Ekstrom S., Maeder A., Georgy C., Eggenberger P., Chiappini C., 2010, A&A, 521, A30
Molaro P., Bonifacio P., Centurión M., D'Odorico S., Vladilo G., Santin P., Di Marcantonio P., 2000, ApJ, 541, 54
Morton D. C., 2003, ApJS, 149, 205
Murphy M. T., Curran S. J., Webb J. K., Ménager H., Zych B. J., 2007, MNRAS, 376, 673
Nissen P. E., Primas F., Asplund M., Lambert D. L., 2002, A&A, 390, 235
Nissen P. E., Akerman C., Asplund M., Fabbian D., Kerber F., Kaufl H. U., Pettini M., 2007, A&A, 469, 319
Norris J. E., Christlieb N., Korn A. J., Eriksson K., Bessell M. S., Beers T. C., Wisotzki L., Reimers D., 2007, ApJ, 670, 774
Noterdaeme P., Ledoux C., Petitjean P., Srianand R., 2008, A&A, 481, 327
Noterdaeme P., Petitjean P., Ledoux C., Srianand R., 2009, A&A, 505, 1087
O'Meara J. M., Burles S., Prochaska J. X., Prochter G., Bernstein R., 2005, in Williams P., Shu C.-G., Menard B., eds, Proc. IAU Symp. 199, Chemical History at $z \geq 2.0$: First Results from the Magellan+Keck Survey of Lyman Limit Systems. Cambridge University Press, Cambridge, p. 463
O'Meara J. M., Burles S., Prochaska J. X., Prochter G. E., Bernstein R. A., Burgess K. M., 2006, ApJ, 649, L61
Oppenheimer B. D., Davé R., 2008, MNRAS, 387, 577
Penprase B. E., Sargent W. L. W., Martinez I. T., Prochaska J. X., Beeler D. J., 2008, in O'Shea B. W., Heger A., Abel T., eds, AIP Conf. Proc. Vol. 990, First Stars III. Am. Inst. Phys., New York, p. 499
Penprase B. E., Prochaska J. X., Sargent W. L. W., Toro-Martinez I., Beeler D. J., 2010, ApJ, 721, 1
Péroux C., Storrie-Lombardi L. J., McMahon R. G., Irwin M., Hook I. M., 2001, AJ, 121, 1799
Péroux C., McMahon R. G., Storrie-Lombardi L. J., Irwin M. J., 2003a, MNRAS, 346, 1103
Péroux C., Dessauges-Zavadsky M., D'Odorico S., Kim T.-S., McMahon R. G., 2003b, MNRAS, 345, 480
Péroux C., Dessauges-Zavadsky M., D'Odorico S., Sun Kim T., McMahon R. G., 2005, MNRAS, 363, 479
Petitjean P., Ledoux C., Srianand R., 2008, A&A, 480, 349
Pettini M., King D. L., Smith L. J., Hunstead R. W., 1997, ApJ, 478, 536
Pettini M., Zych B. J., Steidel C. C., Chaffee F. H., 2008, MNRAS, 385, 2011
Pontzen A. et al., 2008, MNRAS, 390, 1349
Prochaska J. X., 2006, ApJ, 650, 272
Prochaska J. X., Wolfe A. M., 2002, ApJ, 566, 68
Prochaska J. X., Wolfe A. M., 2009, ApJ, 696, 1543
Prochaska J. X., Henry R. B. C., O'Meara J. M., Tytler D., Wolfe A. M., Kirkman D., Lubin D., Suzuki N., 2002, PASP, 114, 933
Prochaska J. X., Gawiser E., Wolfe A. M., Cooke J., Gelino D., 2003, ApJS, 147, 227
Prochaska J. X., Wolfe A. M., Howk J. C., Gawiser E., Burles S. M., Cooke J., 2007, ApJS, 171, 29
Prochaska J. X., Chen H.-W., Wolfe A. M., Dessauges-Zavadsky M., Bloom J. S., 2008, ApJ, 672, 59
Ryan S. G., Aoki W., Norris J. E., Beers T. C., 2005, ApJ, 635, 349
Simcoe R. A., Sargent W. L. W., Rauch M., 2004, ApJ, 606, 92
Spite M. et al., 2005, A&A, 430, 655
Srianand R., Gupta N., Petitjean P., Noterdaeme P., Ledoux C., 2010, MNRAS, 405, 1888
Suda T. et al., 2008, PASJ, 60, 1159
Tescari E., Viel M., Tornatore L., Borgani S., 2009, MNRAS, 397, 411
Tomkin J., Lemke M., Lambert D. L., Sneden C., 1992, AJ, 104, 1568
Tsujimoto T., Bekki K., 2011, A&A, 530, 78
Umeda H., Nomoto K., 2002, ApJ, 565, 385
Umeda H., Nomoto K., 2003, Nat, 422, 871
Vladilo G., 2002, A&A, 391, 407
Vladilo G., 2004, A&A, 421, 479
Vladilo G., Centurión M., Bonifacio P., Howk J. C., 2001, ApJ, 557, 1007
Vogt S. S. et al., 1994, in Crawford D. L., Craine E. R., eds, Proc. SPIE Vol. 2198, Instrumentation in Astronomy VIII. SPIE, Bellingham, p. 362
Wheeler J. C., Sneden C., Truran J. W., Jr, 1989, ARA&A, 27, 279
Wolfe A. M., Turnshek D. A., Smith H. E., Cohen R. D., 1986, ApJS, 61, 249
Wolfe A. M., Gawiser E., Prochaska J. X., 2005, ARA&A, 43, 861

APPENDIX A: VMP DLA COLUMN DENSITIES

To facilitate comparison with future data sets, Table A1 lists ion column densities for the DLAs considered in this study. The corresponding element abundances are collected in Table 11.

APPENDIX B: OXYGEN AND IRON IN DLAS AND STARS

In Tables B1 and B2, we list the values of [O/Fe] and [Fe/H] plotted in Fig. 11 for DLAs and Galactic stars, respectively, together with the corresponding errors. The stellar measurements are all from the [O I] λ6300 line (taken from Nissen et al. 2002; Cayrel et al. 2004; García Pérez et al. 2006), with appropriate 3D corrections based on the work by Nissen et al. (2002) and Collet et al. (2007) (see text in Section 6.2 for further details).

Table A1. C, N, O, Al, Si and Fe column densities in VMP DLAs.

QSO	z_{abs}	log N(H I) (cm^{-2})	log N(C II) (cm^{-2})	log N(N I) (cm^{-2})	log N(O I) (cm^{-2})	log N(Al II) (cm^{-2})	log N(Si II) (cm^{-2})	log N(Fe II) (cm^{-2})	Ref.[a]
Our metal-poor DLA sample									
J0035−0918	2.34010	20.55 ± 0.10	15.47 ± 0.15	13.51 ± 0.06	14.96 ± 0.08	11.73 ± 0.05	13.41 ± 0.04	12.98 ± 0.07	2
J0311−1722	3.73400	20.30 ± 0.06	14.02 ± 0.08	≤13.07	14.70 ± 0.08	...	13.31 ± 0.07	≤13.76	1
J0831+3358	2.30364	20.25 ± 0.15	...	≤12.78	14.93 ± 0.05	12.19 ± 0.06	13.75 ± 0.04	13.33 ± 0.06	1,4
Q0913+072	2.61843	20.34 ± 0.04	13.98 ± 0.05	12.29 ± 0.12	14.63 ± 0.01	11.78 ± 0.03	13.30 ± 0.01	12.99 ± 0.01	3
J1001+0343	3.07841	20.21 ± 0.05	13.58 ± 0.02	≤12.50	14.25 ± 0.02	...	12.86 ± 0.01	12.50 ± 0.14	1
J1016+4040	2.81633	19.90 ± 0.11	13.66 ± 0.04	≤12.76	14.13 ± 0.03	...	12.90 ± 0.05	...	3
J1037+0139	2.70487	20.50 ± 0.08	...	13.27 ± 0.04	15.06 ± 0.04	12.32 ± 0.03	13.97 ± 0.03	13.53 ± 0.02	1
J1340+1106	2.50792	20.09 ± 0.05	...	12.80 ± 0.04	15.02 ± 0.03	12.27 ± 0.02	13.75 ± 0.02	13.49 ± 0.02	1
J1340+1106	2.79583	21.00 ± 0.06	...	14.04 ± 0.02	16.04 ± 0.04	13.24 ± 0.03	14.68 ± 0.02	14.32 ± 0.01	1
J1419+0829	3.04973	20.40 ± 0.03	...	13.28 ± 0.02	15.17 ± 0.02	...	13.83 ± 0.01	13.54 ± 0.03	1
J1558+4053	2.55332	20.30 ± 0.04	14.22 ± 0.06	12.66 ± 0.07	14.54 ± 0.04	11.92 ± 0.06	13.32 ± 0.02	13.07 ± 0.06	3
Q2206−199	2.07624	20.43 ± 0.04	14.41 ± 0.03	12.79 ± 0.05	15.05 ± 0.03	12.18 ± 0.01	13.65 ± 0.01	13.33 ± 0.01	3
Literature DLAs									
Q0000−2620	3.39012	21.41 ± 0.08	...	14.70 ± 0.02	16.42 ± 0.10	...	15.06 ± 0.02	14.87 ± 0.03	5
Q0112−306	2.41844	20.50 ± 0.08	...	13.16 ± 0.04	14.95 ± 0.08	...	13.62 ± 0.02	13.33 ± 0.05	6
J0140−0839	3.69660	20.75 ± 0.15	14.13 ± 0.08	≤12.38	14.69 ± 0.01	11.82 ± 0.04	13.51 ± 0.09	12.77 ± 0.19[b]	7
J0307−4945	4.46658	20.67 ± 0.09	...	13.57 ± 0.12	15.91 ± 0.17	13.36 ± 0.06	14.68 ± 0.07	14.21 ± 0.17	8
Q1108−077	3.60767	20.37 ± 0.07	...	≤12.84	15.37 ± 0.03	...	14.34 ± 0.02	13.88 ± 0.02	6
J1337+3153	3.16768	20.41 ± 0.15	13.98 ± 0.06	≤12.80	14.43 ± 0.09	12.00 ± 0.05	13.24 ± 0.05	13.14 ± 0.26	9
J1558−0031	2.70262	20.67 ± 0.05	...	14.46[c]	15.86[c]	...	14.24[c]	14.11[c]	10
Q1946+7658	2.84430	20.27 ± 0.06	...	12.59 ± 0.04	14.82 ± 0.01	...	13.60 ± 0.01	13.24 ± 0.01	11
Q2059−360	3.08293	20.98 ± 0.08	...	13.95 ± 0.02	16.09 ± 0.04	...	14.86 ± 0.05	14.48 ± 0.02	6
J2155+1358	4.21244	19.61 ± 0.10	13.95 ± 0.06	...	14.50 ± 0.05	11.92 ± 0.17	13.25 ± 0.04	12.93 ± 0.23	12

[a]References – 1: This work; 2: Cooke et al. (2011); 3: Pettini et al. (2008); 4: Penprase et al. (2010); 5: Molaro et al. (2000); 6: Petitjean et al. (2008); 7: Ellison et al. (2010); 8: Dessauges-Zavadsky et al. (2001); 9: Srianand et al. (2010); 10: O'Meara et al. (2006); 11: Prochaska et al. (2002); 12: Dessauges-Zavadsky et al. (2003).

[b]Ellison et al. (2010) quote a 3σ upper limit to the Fe II column density of log N(Fe II)/cm^{-2} < 12.73. We have since rereduced these data (as described in Section 2), and detected the Fe II λ1608 line at the 4σ level. The column density for Fe II quoted here is derived using the optically thin limit approximation.

[c]An error estimate for this measurement was not provided by the authors.

Table B1. [Fe/H] and [O/Fe] in VMP DLAs.

QSO name	z_{abs}	log N(H I) (cm^{-2})	[Fe/H]	[O/Fe]	Ref.[a]
Q0000−2620	3.39012	21.41 ± 0.08	−2.01 ± 0.09	+0.33 ± 0.10	2
J0035−0918	2.34010	20.55 ± 0.10	−3.04 ± 0.12	+0.76 ± 0.11	3
Q0112−306	2.41844	20.50 ± 0.08	−2.64 ± 0.09	+0.40 ± 0.09	4
J0140−0839	3.69660	20.75 ± 0.15	−3.45 ± 0.24	+0.70 ± 0.19	5
J0307−4945	4.46658	20.67 ± 0.09	−1.93 ± 0.19	+0.48 ± 0.24	6
J0311−1722	3.73400	20.30 ± 0.06	≤−2.03	≥−0.26	1
J0831+3358	2.30364	20.25 ± 0.15	−2.39 ± 0.16	+0.38 ± 0.08	1,7
Q0913+072	2.61843	20.34 ± 0.04	−2.82 ± 0.04	+0.42 ± 0.02	8
J1001+0343	3.07841	20.21 ± 0.05	−3.18 ± 0.15	+0.53 ± 0.14	1
J1037+0139	2.70487	20.50 ± 0.08	−2.44 ± 0.08	+0.31 ± 0.04	1
Q1108−077	3.60767	20.37 ± 0.07	−1.96 ± 0.07	+0.27 ± 0.04	4
J1337+3153	3.16768	20.41 ± 0.15	−2.74 ± 0.30	+0.07 ± 0.28	9
J1340+1106	2.50792	20.09 ± 0.05	−2.07 ± 0.05	+0.31 ± 0.04	1
J1340+1106	2.79583	21.00 ± 0.06	−2.15 ± 0.06	+0.50 ± 0.04	1
J1419+0829	3.04973	20.40 ± 0.03	−2.33 ± 0.04	+0.41 ± 0.04	1
J1558−0031	2.70262	20.67 ± 0.05	−2.03[b]	+0.53[b]	10
J1558+4053	2.55332	20.30 ± 0.04	−2.70 ± 0.07	+0.25 ± 0.07	8
Q1946+7658	2.84430	20.27 ± 0.06	−2.50 ± 0.06	+0.36 ± 0.02	11
Q2059−360	3.08293	20.98 ± 0.08	−1.97 ± 0.08	+0.39 ± 0.04	4
J2155+1358	4.21244	19.61 ± 0.10	−2.15 ± 0.25	+0.35 ± 0.24	12
Q2206−199	2.07624	20.43 ± 0.04	−2.57 ± 0.04	+0.50 ± 0.03	8

[a]References – 1: This work; 2: Molaro et al. (2000); 3: Cooke et al. (2011); 4: Petitjean et al. (2008); 5: Ellison et al. (2010); 6: Dessauges-Zavadsky et al. (2001); 7: Penprase et al. (2010); 8: Pettini et al. (2008); 9: Srianand et al. (2010); 10: O'Meara et al. (2006); 11: Prochaska et al. (2002); 12: Dessauges-Zavadsky et al. (2003).

[b]An error estimate for this measurement was not provided by the authors.

Table B2. [Fe/H] and [O/Fe] in metal-poor stars.

Star Name	$T_{\rm eff}$ [a] (K)	$\log g$ [b] (cgs)	[Fe/H]	[O/Fe]	Ref.[c]
HD 2796	4950	1.50	-2.37 ± 0.10	$+0.23 \pm 0.13$	1
HD 3567	6000	4.07	-1.11 ± 0.06	$+0.29 \pm 0.06$	2
HD 4306	4990	3.04	-2.24 ± 0.10	$+0.47 \pm 0.11$	3
HD 26169	4972	2.49	-2.19 ± 0.10	$+0.34 \pm 0.09$	3
HD 27928	5044	2.67	-2.05 ± 0.10	$+0.22 \pm 0.11$	3
HD 45282	5352	3.15	-1.46 ± 0.10	$+0.33 \pm 0.07$	3
HD 97320	5976	4.16	-1.16 ± 0.06	$+0.20 \pm 0.12$	2
HD 108317	5300	2.76	-2.16 ± 0.10	$+0.49 \pm 0.12$	3
HD 111980	5694	3.99	-1.03 ± 0.06	$+0.17 \pm 0.07$	2
HD 122563	4600	1.10	-2.71 ± 0.10	$+0.31 \pm 0.13$	1
HD 126587	4712	1.66	-2.76 ± 0.10	$+0.13 \pm 0.14$	3
HD 126681	5524	4.48	-1.12 ± 0.06	$+0.33 \pm 0.08$	2
HD 128279	5336	2.95	-2.10 ± 0.10	$+0.17 \pm 0.23$	3
HD 132475	5818	3.95	-1.39 ± 0.06	$+0.33 \pm 0.09$	2
HD 140283	5690	3.69	-2.32 ± 0.06	$+0.50 \pm 0.19$	2
HD 160617	5931	3.77	-1.72 ± 0.06	$+0.22 \pm 0.15$	2
HD 166913	6039	4.11	-1.50 ± 0.06	$+0.22 \pm 0.24$	2
HD 186478	4700	1.30	-2.49 ± 0.10	$+0.47 \pm 0.10$	1
HD 189558	5613	3.91	-1.07 ± 0.06	$+0.31 \pm 0.05$	2
HD 205650	5733	4.39	-1.12 ± 0.06	$+0.30 \pm 0.09$	2
HD 213657	6114	3.85	-1.86 ± 0.06	$+0.30 \pm 0.24$	2
HD 218857	5015	2.78	-1.72 ± 0.10	$+0.18 \pm 0.09$	3
HD 274939	5090	2.79	-1.43 ± 0.10	$+0.35 \pm 0.05$	3
HD 298986	6071	4.21	-1.30 ± 0.06	$+0.23 \pm 0.17$	2
BD -18°5550	4750	1.40	-2.94 ± 0.10	$+0.08 \pm 0.24$	1
BD -01°2582	5072	2.92	-2.03 ± 0.10	$+0.31 \pm 0.11$	3
BD $+17^\circ$3248	5250	1.40	-1.99 ± 0.10	$+0.46 \pm 0.11$	1
BD $+23^\circ$3130	5170	3.00	-2.29 ± 0.06	$+0.38 \pm 0.15$	2
CS 22186 − 035	4900	1.50	-2.88 ± 0.10	$+0.26 \pm 0.26$	1
CS 22873 − 055	4550	0.70	-2.87 ± 0.10	$+0.19 \pm 0.13$	1
CS 22891 − 209	4700	1.00	-3.16 ± 0.10	$+0.41 \pm 0.16$	1
CS 22892 − 052	4850	1.60	-2.91 ± 0.10	$+0.14 \pm 0.26$	1
CS 22896 − 154	5250	2.70	-2.58 ± 0.10	$+0.64 \pm 0.23$	1
CS 22948 − 066	5100	1.80	-3.01 ± 0.10	$+0.54 \pm 0.23$	1
CS 22949 − 037	4900	1.50	-3.81 ± 0.10	$+1.54 \pm 0.13$	1
CS 22953 − 003	5100	2.30	-2.73 ± 0.10	$+0.44 \pm 0.23$	1
CS 22966 − 057	5300	2.20	-2.52 ± 0.10	$+0.70 \pm 0.20$	1
CS 22968 − 014	4850	1.70	-3.42 ± 0.10	$+0.51 \pm 0.27$	1
CS 29491 − 053	4700	1.30	-2.92 ± 0.10	$+0.43 \pm 0.17$	1
CS 29495 − 041	4800	1.50	-2.71 ± 0.10	$+0.37 \pm 0.13$	1
CS 29516 − 024	4650	1.20	-2.94 ± 0.10	$+0.28 \pm 0.20$	1
CS 29518 − 051	5200	2.60	-2.58 ± 0.10	$+0.63 \pm 0.23$	1
CS 30325 − 094	4950	2.00	-3.17 ± 0.10	$+0.36 \pm 0.33$	1
CS 31082 − 001	4825	1.50	-2.79 ± 0.10	$+0.28 \pm 0.15$	1

[a] Stellar effective temperature.
[b] Surface gravity.
[c] References – 1: Cayrel et al. (2004); 2: Nissen et al. (2002); 3: García Pérez et al. (2006).

This paper has been typeset from a TEX/LATEX file prepared by the author.